

FINAL REPORT

Demonstration of LiDAR and Orthophotography for Wide
Area Assessment at Pueblo Precision Bombing Range
#2, Colorado

ESTCP Project MM-0416 and MM-0535

JANUARY 2008

Dr. Jack Foley
Sky Research, Inc.

Approved for public release; distribution
unlimited.



Environmental Security Technology
Certification Program

Report Documentation Page				Form Approved OMB No. 0704-0188	
Public reporting burden for the collection of information is estimated to average 1 hour per response, including the time for reviewing instructions, searching existing data sources, gathering and maintaining the data needed, and completing and reviewing the collection of information. Send comments regarding this burden estimate or any other aspect of this collection of information, including suggestions for reducing this burden, to Washington Headquarters Services, Directorate for Information Operations and Reports, 1215 Jefferson Davis Highway, Suite 1204, Arlington VA 22202-4302. Respondents should be aware that notwithstanding any other provision of law, no person shall be subject to a penalty for failing to comply with a collection of information if it does not display a currently valid OMB control number.					
1. REPORT DATE 01 JAN 2008		2. REPORT TYPE N/A		3. DATES COVERED -	
4. TITLE AND SUBTITLE Demonstration of LiDAR and Orthophotography for Wide Area Assessment at Pueblo Precision Bombing Range #2, Colorado				5a. CONTRACT NUMBER	
				5b. GRANT NUMBER	
				5c. PROGRAM ELEMENT NUMBER	
6. AUTHOR(S)				5d. PROJECT NUMBER	
				5e. TASK NUMBER	
				5f. WORK UNIT NUMBER	
7. PERFORMING ORGANIZATION NAME(S) AND ADDRESS(ES) Sky Research, Inc.				8. PERFORMING ORGANIZATION REPORT NUMBER	
9. SPONSORING/MONITORING AGENCY NAME(S) AND ADDRESS(ES)				10. SPONSOR/MONITOR'S ACRONYM(S)	
				11. SPONSOR/MONITOR'S REPORT NUMBER(S)	
12. DISTRIBUTION/AVAILABILITY STATEMENT Approved for public release, distribution unlimited					
13. SUPPLEMENTARY NOTES The original document contains color images.					
14. ABSTRACT					
15. SUBJECT TERMS					
16. SECURITY CLASSIFICATION OF:			17. LIMITATION OF ABSTRACT UU	18. NUMBER OF PAGES 71	19a. NAME OF RESPONSIBLE PERSON
a. REPORT unclassified	b. ABSTRACT unclassified	c. THIS PAGE unclassified			

TABLE OF CONTENTS

Table of Contents.....	i
Acronyms.....	iv
Acknowledgments	vi
1. Introduction.....	1
1.1 Background.....	1
1.2 Objectives of the Demonstration	2
1.3 Regulatory Drivers.....	2
1.4 Stakeholder/End User	2
2. Technology Description.....	3
2.1 Technology Development and Application	3
2.1.1 Fixed-Wing Platform	3
2.1.2 LiDAR System.....	4
2.1.3 LiDAR Data Processing.....	5
2.1.4 Orthophotography System	5
2.1.5 Orthophotography Data Processing	7
2.1.6 Data Analysis	7
2.2 Previous Testing of the Technology	8
2.3 Factors Affecting Cost and Performance.....	8
2.4 Advantages and Limitations of the Technology	9
3. Demonstration Design	10
3.1 Performance Objectives	10
3.2 Test Site Selection.....	11
3.3 Test Site History/Characteristics.....	11
3.4 Pre-Demonstration Testing and Analysis	15
3.5 Testing and Evaluation Plan	17
3.5.1 Demonstration Set-Up and Start-Up.....	17
3.5.2 Crater Emplacement.....	17
3.5.3 Ground Control	18
3.5.4 Navigation Systems	19
3.5.5 Period of Operation.....	20
3.5.6 Operating Parameters for the Technology	20
3.5.7 Demobilization.....	21
3.6 Data Processing.....	23
3.6.1 LiDAR Data Processing.....	23
3.6.2 Orthophotography Data Processing	24

3.7. Data Analysis	26
3.7.1. Computation of Derivative LiDAR Images	27
3.7.2. Image Analysis Grids.....	27
3.7.3. Target Feature Identification and Extraction	27
3.7.4. Crater Feature Identification and Extraction.....	28
3.7.5. Range Infrastructure Identification and Extraction.....	30
4. Performance Assessment	31
4.1 Crater Detection Analysis	31
4.2 Spatial Accuracy	34
4.2.1 LiDAR Data Spatial Accuracy.....	34
4.2.2 Orthophotography Data Spatial Accuracy	35
4.3 Data Analysis Results	35
4.3.1 Target Area Detection.....	35
4.3.2 Crater Detection	43
4.3.3 Range Infrastructure Detection	47
4.4 Performance Criteria.....	49
4.5 Performance Confirmation Methods.....	49
4.5.1 Technology Usage	50
4.5.2 Georeference Accuracy.....	51
4.5.3 Target Area Detection.....	51
4.5.4 Detection of Potential Craters	51
4.5.5 Range Infrastructure Detection	51
5. Cost Assessment	54
5.1 Cost Reporting	54
5.2 Cost Analysis	57
6. Implementation Issues	58
6.1 Regulatory and End-User Issues.....	58
7. References.....	59
8. Points of Contact.....	60
Appendix A: Optech ALTM 3100 Specifications	A-1
Appendix B: ALTM 4K X 4K Digital Camera Specifications.....	B-1
Appendix C: Feature Database and Attribute Summary	C-1

LIST OF FIGURES

Figure 1. C208 fixed-wing platform houses the orthophotography and LiDAR sensors for concurrent data collection.	3
Figure 2. The WAA demonstration area (in yellow) is located within the former Pueblo Precision Bombing Range in Otero County, Colorado.....	12
Figure 3. LiDAR and orthophotography data collection was conducted in two phases, with Phase I data collection in 2004, and Phase II data collection in 2005.	13
Figure 4. Crater calibration area at Sky Research calibration area in Ashland, Oregon.	16
Figure 5. Example of a calibration site crater with a diameter of 0.75 m and depth of 0.4 m.....	16
Figure 6. LiDAR ground fiducial (left) and orthophotography aerial target (right).....	18
Figure 7. Ground fiducial emplacement for Phase I and Phase II data collection at Pueblo PBR#2.	19
Figure 8. Phase I orthophotography data collection boundaries.....	22
Figure 9. Phase II orthophotography data collection boundaries.	22
Figure 10. Screenshot of ISAT aerotriangulation results window.....	25
Figure 11. Screenshot of OrthoPro seam lines (pink), tiles (blue), and photos (green).....	26
Figure 12. Calibration craters (existing), hillshade image.....	32
Figure 13. Calibration craters (existing), analytic image.....	32
Figure 14. Calibration craters (emplaced), hillshade image.	33
Figure 15. Calibration craters (emplaced), analytic image.....	33
Figure 16. LiDAR spatial accuracy assessment methodology.....	34
Figure 17. Orthophotography spatial accuracy assessment methodology.	35
Figure 18. BT3 target circle as detected in orthophotography (top) and LiDAR (bottom) imagery.	37
Figure 19. Delineation of target features at BT3 and vicinity.	38
Figure 20. Partial ship outline at BT3, located on the western side of aiming circle.	39
Figure 21. Raised features identified north of BT3 target circle.	39
Figure 22. BT4 aiming circle with crosshairs delineated.	40
Figure 23. Four ship targets were detected in the LiDAR imagery in the vicinity of BT4.	41
Figure 24. Ship target at BT4 feature as overlain on LiDAR hillshade (top left); HSI (top right), orthophotography (bottom left) and LiDAR high-pass (bottom right) imagery.....	42
Figure 25. No munitions related features were detected within the boundaries of the Suspected 75 mm Target Area (1995 ASR boundaries).	43
Figure 26. Potential craters detected at BT3.....	44

Figure 27. Potential crater density analysis at BT4.	46
Figure 28. Possible range infrastructure features detected in the imagery includes transport routes (white lines); building structure and foundation pad.	48

LIST OF TABLES

Table 1. LiDAR Specifications.....	4
Table 2. Camera Specifications	6
Table 3. Primary Performance Objectives	10
Table 4. Secondary Performance Objectives	11
Table 5. Acquisition Parameters for LiDAR Surveys at Pueblo PBR#2.....	21
Table 6. Color Orthophotography Data Acquisition Parameters.....	21
Table 7. Diagnostic Detectability of Crater Features in LiDAR Imagery	31
Table 8. LiDAR Data Accuracy Results.....	34
Table 9. Orthophotography Data Accuracy Results	35
Table 10. Performance Criteria.....	49
Table 11. Performance Confirmation Methods and Results.....	50
Table 12. Crater Detection Comparison to Validation Data.....	52
Table 13. Phase I Cost Tracking	54
Table 14. Phase II Cost Tracking.....	55
Table 15. Points of Contact.....	60

ACRONYMS

3D	Three Dimensional
AAF	Army Air Force
AGL	Above Ground Level
ASR	Archive Search Report
BT3	Bomb Target 3
BT4	Bomb Target 4
C	Celsius
C208	Cessna 208
CCD	Charged Coupled Device
CFR	Code of Federal Regulations
CERCLA	Comprehensive Environmental, Response, Compensation, and Liability Act
cm	centimeter(s)
CSM	Conceptual Site Model
DEM	Digital Elevation Model
DTM	Digital Terrain Model
DoD	Department of Defense
DSB	Defense Science Board
DTM	Digital Terrain Model
ESRI	Environmental Systems Research Institute
ESTCP	Environmental Security Technology Certification Program
FOV	Field of View
FLBGR	Former Lowry Bombing and Gunnery Range
FUDS	Formerly Used Defense Sites
GIS	Geographic Information Systems
GB	gigabyte
GPS	Global Positioning System
GSD	Ground Sample Distance
HE	High Explosive
Hz	Hertz
ID	Identification
IDL	Interactive Data Language
IMU	Inertial Measurement Unit
ISAT	ImageStation Auto Triangulation
kHz	kilohertz
km	kilometer(s)
LiDAR	Light Detection and Ranging
m	meter(s)
mm	millimeter(s)
MMRP	Military Munitions Response Program
MNF	Minimum Noise Fraction
MRF	Munitions Related Feature
MRA	Munitions Response Area
NAD83	1983 North American Datum
NE	Northeast

OB/OD	Open Burn/Open Detonation
PDOP	Position Dilution of Precision
POS	Position and Orientation
PBR	Precision Bombing Range
RGB	Red-Green-Blue
RMSE	Root Mean Square Error
RTK GPS	Real-time Kinematic GPS
SBET	Smooth Best Estimate Trajectory
SDE	Spatial Database Engine
SW	Southwest
USACE	United States Army Corps of Engineers
UTM	Universal Transverse Mercator
UXO	Unexploded Ordnance
WAA	Wide Area Assessment
WAA-PP	Wide Area Assessment Pilot Program

ACKNOWLEDGMENTS

Demonstration of LiDAR and Orthophotography for Wide Area Assessment at Pueblo Precision Bombing Range #2, Colorado, documents the acquisition, processing, analysis, and interpretation of high airborne LiDAR and orthophotography data for wide area assessment at the former Pueblo Precision Bombing Range #2. The work was performed by Sky Research, Inc. of Oregon, with Dr. John Foley serving as Principal Investigator.

Funding for this project was provided by the Environmental Security Technology Certification Program Office. This project offered the opportunity to examine advanced airborne methods as part of the Department of Defense's efforts to evaluate wide area assessment technologies for efficient the characterization and investigation of large Department of Defense sites.

We wish to express our sincere appreciation to Dr. Jeffrey Marqusee, Dr. Anne Andrews, and Ms. Katherine Kaye of the ESTCP Office for providing support and funding for this project.

1. Introduction

1.1 Background

Unexploded ordnance (UXO) contamination is a high-priority problem for the Department of Defense (DoD). Recent DoD estimates of UXO contamination across approximately 1,400 DoD sites indicate that 10 million acres are suspected of containing UXO. Because many sites are large in size (greater than 10,000 acres), the investigation and remediation of these sites could cost billions of dollars. However, on many of these sites only a small percentage of the site may in fact contain UXO contamination. Therefore, determining applicable technologies to define the contaminated areas requiring further investigation and munitions response actions could provide significant cost savings. Therefore, the Defense Science Board (DSB) has recommended further investigation and use of Wide Area Assessment (WAA) technologies to address the potential these technologies offer in terms of determining the actual extent of UXO contamination on DoD sites (DSB, 2003).

In response to the DSB Task Force report and recent Congressional interest, the Environmental Security Technology Certification Program (ESTCP) designed a Wide Area Assessment Pilot Program (WAA-PP) that consists of demonstrations at multiple sites to validate the application of a number of recently developed and validated technologies as a comprehensive approach to WAA. These demonstrations of WAA technologies include deployment of high airborne sensors, helicopter-borne magnetometry arrays and ground surveys.

This report describes the data collection, methodology and analysis conducted by Sky Research for the following high airborne sensor technologies demonstrated at Pueblo Precision Bombing Range (PBR) #2 in Otero County, Colorado: Light Detection and Ranging (LiDAR) and orthophotography. LiDAR data are critical to the overall WAA process in several roles: creation of an accurate high-resolution bare earth digital elevation model (DEM) for ortho-correction of all other remote-sensing datasets; extraction of possible surface munitions related features (MRFs) and for base mapping layers for site visualization, planning and analysis. Orthophotography is valuable for direct detection and visualization of possible MRFs; as input to

multiple-sensor fusion algorithms for surface feature detection; and for site visualization and planning.

1.2 Objectives of the Demonstration

The LiDAR and orthophotography demonstration was conducted to determine the utility of these data sets to achieve the following objectives: identification of munitions related features including two documented bombing targets (Bombing Targets #3 and #4 [BT3 and BT4]) and a suspected 75 mm air-to-ground gunnery target area, characterization of site conditions for additional site investigation (i.e., low airborne and ground surveys), and planning and remediation.. The location of the air-to-ground gunnery target area was identified as having a high level of uncertainty as it had been identified through a third-hand report of the finding of a 75 mm round by a landowner, and there was contradictory evidence that suggested the 75 mm range was located outside of the study area in another part of the munitions response area (MRA) (U.S. Army Corps of Engineers, 1995).

1.3 Regulatory Drivers

United States Army Corps of Engineers (USACE) is the lead federal agency under the Formerly Used Defense Site (FUDS) program. USACE administers the FUDS Military Munitions Response Program (MMRP) program using DoD investigation/cleanup methods based on the U.S. Environmental Protection Agency Comprehensive Environmental, Response, Compensation, and Liability Act (CERCLA) process.

1.4 Stakeholder/End User

ESTCP is managing the stakeholder issues as part of its WAA-PP. ESTCP plans to use a process that will ensure that the information generated by the high airborne, helicopter, airborne, ground validation surveys is useful to a broad stakeholder community (e.g., technical project managers and Federal, State, and local governments, as well as other stakeholders).

2. Technology Description

2.1 Technology Development and Application

Airborne sensors utilized for this demonstration are based on existing, well-developed airborne remote sensing technologies. The Phase I and II data collections, processing and analysis systems used for this demonstration include a fixed-wing plane platform housing the data acquisition technologies and a suite of data processing and analysis software.

2.1.1 Fixed-Wing Platform

The ALTM 3100 LiDAR system, ALTM 4K02 Digital Metric Camera, and the Position and Orientation System (POS) were mounted in the Sky Research Cessna 208 (C208) Caravan aircraft (Figure 1). The C208 is an unpressurized single-engine high wing turboprop with fixed landing gear. A removable composite cargo pod provides housing for the equipment and sensors; both the LiDAR and orthophotography sensors were installed to allow for concurrent data collection.

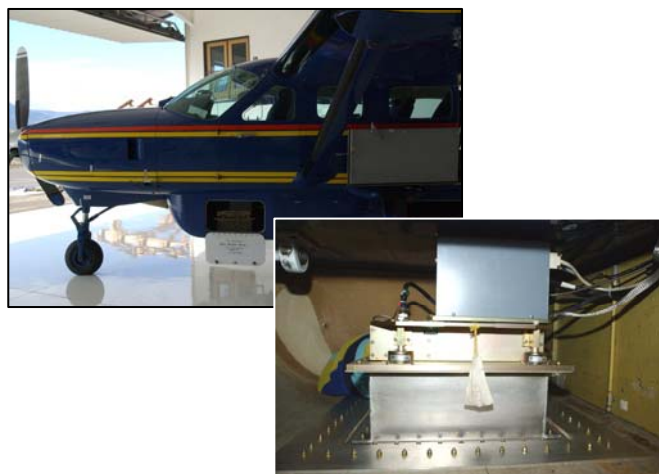


Figure 1. C208 fixed-wing platform houses the orthophotography and LiDAR sensors for concurrent data collection.

2.1.2 LiDAR System

The LiDAR data collection system – comprised of an Optech ALTM 3100 laser scanner, global positioning system (GPS), and inertial measurement unit (IMU) – is capable of producing precise high-resolution topographic data. The Optech ALTM 3100 LiDAR sensor specifications are summarized in Table 1 below. For detailed specifications, please see Appendix A.

Table 1. LiDAR Specifications

Detector type:	Optech® LiDAR ALTM 3100
Spacing:	30 centimeters (cm) to 5 meters (m) spot spacing
Contour Interval:	Dependent on spot spacing with an approximate 1 m (spacing) to 30.5 cm (contour interval) ratio
Operating Altitude:	80-3,500 m above ground level (AGL) nominal
Elevation Accuracy:	<15 cm at 1200 m; 1 sigma <25 cm at 2000 m; 1 sigma <35 cm at 3000 m; 1 sigma
Horizontal Accuracy:	Better than 1/3,000 x altitude; 1 sigma
Range Accuracy:	2-3 cm, single shot
Range Resolution:	1 cm
Measurement Rate:	33,000 to 100,000 measurements per second
Scan Angle:	0 to $\pm 25^\circ$
Swath Width:	Variable from 0 to 0.93 x altitude
Scan Frequency:	0-70 Hertz (Hz), depending on scan angle
Laser Classification:	Class IV (FDA Code of Federal Regulations [CFR] 21)
Laser Repetition Rate:	33 kilohertz (kHz) (max. altitude AGL 3500 m) 50 kHz (max. altitude AGL 2500 m) 70 kHz (max. altitude AGL 1700 m) 100 kHz (max. altitude AGL 1100 m)
Operating Temperature:	10-35° Celsius (C)
Humidity:	0-95% non-condensing

The laser scanner operates by emitting high-frequency infrared laser beams. The scanner records the time difference between the emission of the laser pulses and the reception of the reflected signal. A mirror mounted in front of the laser rotates, directing the laser pulses to sweep back and forth perpendicular to the flight direction, which allows the laser scanner to collect swaths of topographic data as the aircraft moves forward. The position of the aircraft is determined by processing differential, dual-frequency, kinematic GPS observations. The GPS located in the aircraft is supported by several ground stations that are located within the vicinity of the acquisition area. The IMU determines the orientation of the aircraft (pitch, roll, and yaw) during

data collection. By combining the IMU data with the post-processed GPS data, the exact trajectory of each laser pulse is determined during data processing.

During data acquisition flights, the sensor operator observes the real-time LiDAR swath coverage to assure full coverage of the survey area. The operator also monitors in-flight Position Dilution of Precision (PDOP) and GPS satellite coverage. If tolerance thresholds of either are exceeded, data acquisition activities are put on hold until acceptable conditions resumed. After the data acquisition flights, data from GPS base stations are checked against in-flight GPS data for concurrence. Once data quality assessments are completed, all data (image and ancillary) are transferred to a centralized location for pre-processing and quality control analysis.

2.1.3 LiDAR Data Processing

Processing of the raw data sets employs a variety of software technologies. Sky Research uses the following technologies:

- POSPac/POSGPS® software for GPS data processing
- POSProc software for combining post-processed GPS data with IMU data
- Optech's REALM software for initial processing and output of LiDAR point cloud data
- Terrasolid's TerraScan software for classification of LiDAR points into vegetation, ground, and "other," creating bare earth and surface model digital terrain models (DTM)
- Environmental Systems Research Institute (ESRI) ArcGIS geoprocessing scripts and Natural Neighbor interpolation for interpolating both DTM models to DEMs and shaded relief imagery
- Visual Learning Systems Feature Analyst ArcGIS extension and custom interactive data language (IDL) software algorithms to locate, detect, and characterize micro-topographic features, including craters.

2.1.4 Orthophotography System

A high-resolution Optech ALTM 4K02 digital metric camera with high-resolution Charged Couple Device (CCD) backing was mounted in the aircraft to capture the aerial photography. This system works as follows: the CCD converts light into electrons, which are enumerated and converted into a digital value. The ability of a CCD to accurately measure and convert the value

of electrons into digital format is the measure of quality. As a small format system, the ALTM4K02 camera used for data collection at the site offers a 36° field of view (FOV) minimizing layback distortion at the edges of images. This feature allows for minimal image distortion during the orthorectification phase of processing. The manufacturer's specifications for the Optech ALTM 3100 4K02 digital metric camera used for data collection are summarized in Table 2; detailed specifications are provided in Appendix B.

Table 2. Camera Specifications

Detector Type:	OPTECH ALTM 4K02 Digital Metric Camera DSS 301 SN0046- 55 millimeters (mm) lens
Lens Type:	Zeiss Distagon
Focal length:	55.073 mm
Field of View:	36°
CCD Specifications:	4,092 (along flight) x 4,079 (cross flight) Pixel size of 0.000138 inches (in)
Shutter Speed:	1/125 to 1/4000 second
Principal Point	Xppac (mm) -0.390, Accuracy 0.0036 Yppac 0.222, Accuracy 0.0036 Measured from image center (pixel size = 9 microns)
Pixel Non-Squareness	1.0, Accuracy 0.0000001
VIS Calibrated Gain Value	0.98
VIS Calibrated ISO	300
VIS Calibrated Exposure Compensation	-0.70

The camera is linked to a computer or a manual trigger device which controls the frequency and length of exposures, resulting in overlapping images. Information collected from the GPS and IMU are used to rectify the aerial photographs. This is accomplished by assigning a geographic coordinate to each image derived from the processing of the GPS data. In addition, distortions created by camera tilt, lens distortion, and terrain displacement are removed to produce an orthophotograph.

During the data acquisition flights, the sensor operator observes the real-time photograph footprint coverage to assure required percentage of overlap for the survey area. The operator observes real-time photo display for verification of image quality. The operator also monitors in-flight PDOP and GPS satellite coverage. If tolerance thresholds of either are exceeded, data acquisition activities are put on hold until acceptable conditions resume. After the data

acquisition flights, data from GPS base stations are checked against in-flight GPS data for concurrence. Once data quality assessments are completed, all data (image and ancillary) are transferred to a centralized location for pre-processing and quality control.

2.1.5 Orthophotography Data Processing

Processing of the raw data sets employs a variety of software technologies. Sky Research uses the following technologies:

- POSPac/POSGPS® software for GPS data processing
- POSProc software for combining post-processed GPS data with IMU data
- Raw photographs developed into TIFF format with manufacturer-calibrated true-color (VIS) filter
- DSS MissionView 2.0 for downloading images from removable drives
- POSEO 4.1 for processing of the photographs to sync with GPS data
- ZI Imaging ImageStation Auto Triangulation (ISAT) software to combine formatted image files with exterior orientation files
- ImageStation OrthoPro software for rectification of the photography to the DTM.

2.1.6 Data Analysis

Once processed, the LiDAR/orthophotography datasets are analyzed to characterize any MRFs that are visible in the datasets and that may be useful in characterizing munitions contamination present at the site. These surface features may include high-explosive craters, target and range berms, burial trenches, abandoned service roads, artillery targets, and other features where a surface topographic or soil/vegetation expression is observed in the LiDAR and/or orthophotography datasets. Extraction of the potential MRFs from the orthophotography and LiDAR datasets is both an automated and analyst-performed task that combines multiple-overlay image interpretation with automated spatial feature recognition processes utilizing ArcGIS and Visual Learning Systems software.

2.2 Previous Testing of the Technology

Component WAA technologies have been developed and tested at a number of defense sites over the past ten years. A WAA at Former Lowry Bombing and Gunnery Range (FLBGR) in Colorado was the first practical application of the use of LiDAR and orthophotography methodology for UXO site assessment. However, at the time the FLBGR WAA was conducted, much of the site had been surface-cleared of munitions contamination at known sites, significantly complicating the analysis.

Since then, demonstrations of LiDAR/orthophotography technologies have been conducted for each demonstration site part of the WAA-PP demonstrations. Preliminary final results demonstrated successful attainment of project goals and objectives, and all sensor systems performed at or above anticipated performance levels (ESTCP 2006).

2.3 Factors Affecting Cost and Performance

One of the most important factors affecting performance of the use of airborne remote sensing for wide area assessment is site phenomenology:

- What type of UXO contamination is present at the site?
- What MRFs exist to indicate the presence of contamination?
- What is the degree of correlation between MRFs and contamination?

Regarding cost, for all airborne surveys, the largest single factor affecting the survey costs is the cost of operating the survey aircraft and sensors at the site. These equipment costs are related to capital value, maintenance overhead and direct operating costs of these expensive sensor and aircraft systems. Mobilization to and from the site increases costs as distance increases, and flexibility of scheduling is critical in determining whether mobilization and deployment costs can be shared across projects. Another significant cost factor is data volume and the requirement for a robust data processing infrastructure to manage large amounts of digital remote sensing data.

2.4 Advantages and Limitations of the Technology

As with all characterization technologies, site specific advantages and disadvantages exist that dictate the level of success of their application. However, in general, the advantages of high airborne sensor WAA technologies include:

- the ability to characterize very large areas;
- WAA site characterization is defined in terms of MRFs, providing a more robust structure to the overall conceptual site model (CSM);
- ability to deploy multiple sensors to increase the opportunity to define MEC contamination; and
- provide significant “value added” features for site characterization. For example, LiDAR / orthophotography technology provides high fidelity DEMs and high resolution photography within a Geographic Information System (GIS) that can be utilized for a wide variety of site activities.

Limitations of the demonstrated WAA technologies include:

- use of high airborne sensors is not intended to detect individual munitions;
- site physiography, such as terrain and vegetation, can constrain the use of technology for MRF detection;
- LiDAR and orthophotography technologies can only detect MRFs with expression on the earth surface; and
- each technology has survey rate and cost versus detection fidelity trade-offs.

3. Demonstration Design

3.1 Performance Objectives

Performance objectives are a critical component of the demonstration plan because they provide the basis for evaluating the performance and costs of the technology. For the LiDAR and orthophotography demonstration at Pueblo PBR#2, both primary and secondary performance objectives have been established. Table 3 lists the primary performance objectives for the high airborne remote sensing technology and Table 4 lists the secondary performance objectives, along with criteria and metrics for evaluation.

Table 3. Primary Performance Objectives

Type of Performance Objective	Primary Performance Criteria	Expected Performance (Metric)	Performance Confirmation Method
Qualitative	Ease of use and efficiency of operations for each sensor system	Efficiency and ease of use meets design specifications	General observations from project team
Quantitative	Georeference position accuracy for each sensor system	LiDAR: Vertical accuracy -15 cm RMSE; Horizontal accuracy - 40 cm RMSE	Comparison of datasets with ground fiducials
		Orthophotography: Horizontal accuracy - 40 cm RMSE	
	Target Area Detection	>0.90 of target areas having topographic aiming point features	Comparison of ortho and LiDAR data analysis results with ground validation data

Table 4. Secondary Performance Objectives

Type of Performance Objective	Primary Performance Criteria	Expected Performance (Metric)	Performance Confirmation Method
Quantitative	Crater Detection	>0.75 (craters <1m) >0.90 (craters >1 m)	Comparison of LiDAR data analysis results with ground validation data
	Range Infrastructure Detection	>0.90	Comparison of ortho and LiDAR data analysis results with ground validation data

3.2 Test Site Selection

This demonstration was originally initiated in 2004 (Phase I) as an ESTCP demonstration project. In response to the DSB Task Force report and Congressional interest, ESTCP created the WAA-PP in 2005 to validate the application of a number of recently developed technologies as a comprehensive approach to WAA. The former Pueblo PBR#2 was selected as a demonstration site based on criteria selected by the ESTCP Program Office in coordination with the WAA advisory group of state and federal regulators. In response to that selection, the demonstration area was expanded and a second data collection (Phase II of this demonstration) was conducted in 2005.

3.3 Test Site History/Characteristics

Pueblo PBR#2 was used as a World War II-era military training facility, located in the southern part of Otero County, Colorado. Within the 105 square-mile (67,770 acres) FUDS, the demonstration area consists of approximately 7,500 acres encompassing two documented bombing targets (Bombing Targets #3 and #4 [BT3 and BT4]) and a suspected 75 mm air-to-ground gunnery target area (Figure 2). Phase I and II data areas are shown in Figure 3. The physiography and known munitions use history of the study area are discussed in some detail in the CSM (Versar, 2005). Physiographic and historic military use characteristics most relevant to the technology demonstration are described briefly in this report.

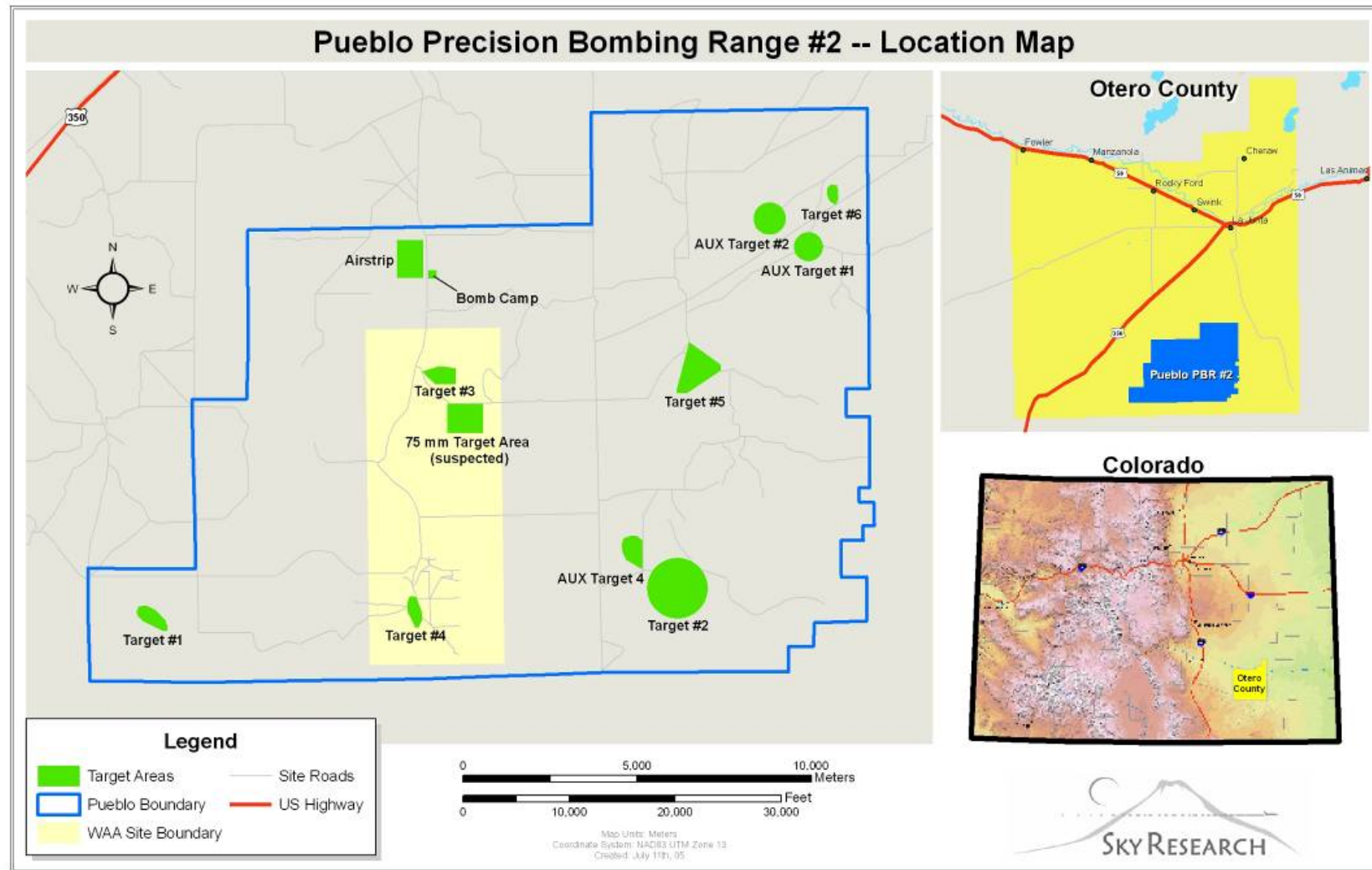


Figure 2. The WAA demonstration area (in yellow) is located within the former Pueblo Precision Bombing Range in Otero County, Colorado.

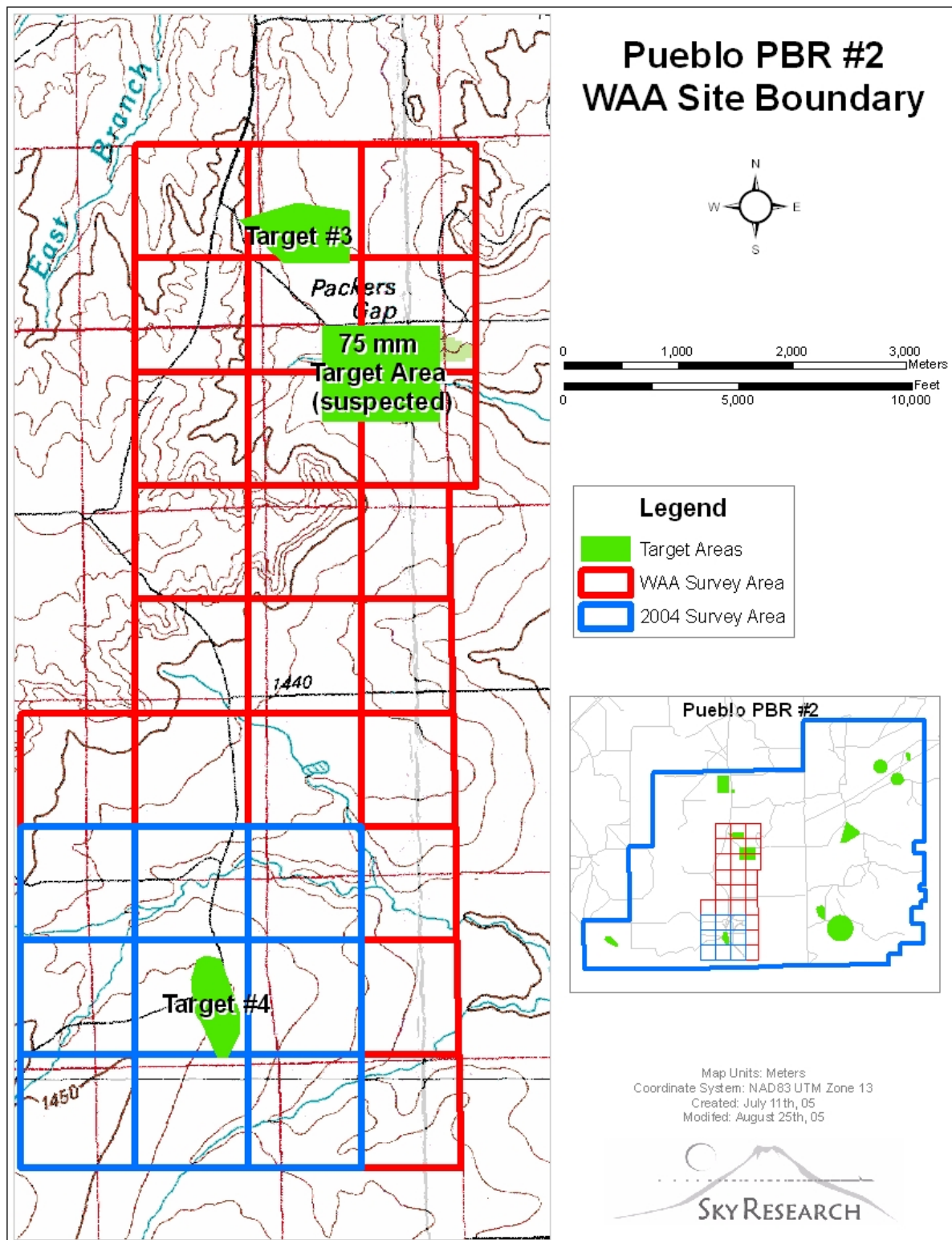


Figure 3. LiDAR and orthophotography data collection was conducted in two phases, with Phase I data collection in 2004, and Phase II data collection in 2005.

Topography. The study area is rolling terraced terrain to the south dissected by several intermittent drainages. The northern half is traversed southwest (SW) to northeast (NE) by an eroded bedrock ridge with a dissected terrace to the northwest. BT4 is on the nose of a gentle rounded ridge, while BT3 is on a steeper slope below and east of the ridge. The suspected 75 mm air-to-ground target area is in a multiple-drainage incised bowl draining the steepest part of the ridge.

Soils and Vegetation. The majority of the site is composed of deep silty sandy clays over silty clay subsoils, on gypsum, marl and limestone parent material. On the ridge, sedimentary bedrock is exposed with poorly developed colluvial soils on the associated slopes. The dominant vegetation is short- and mid-grass prairie dominated by buffalo grass (*Buchloe dactyloides*) and blue grama (*Bouteloua gracilis*), with a mixed overstory of taller native grasses including western wheatgrass and various needlegrass species. Many native forbs are present, and the most common non-herbaceous species include yucca, prickly pear, and cholla. Riparian zones along ephemeral streams on the site are vegetated with sparse riparian scrub and scattered cottonwoods with the understory largely barren due to cattle grazing.

Climate and Hydrology. The climate of the site is characterized by hot dry summers and cold winters. Some of the seasonal precipitation is from winter snows, but strong thunderstorms and associated erosion are the typical spring and summer precipitation pattern. Surface munitions and UXO at the suspected 75 mm air-to-ground target area and BT3 sites are most liable to surface transport and burial by erosion and soil movement associated with these seasonal rainfall events. Similarly, micro-topographic target and impact features at these sites are most subject to obliteration by climatic factors.

Land Use. Land within the study area is primarily in Federal ownership managed by the U.S. Forest Service as the Comanche National Grasslands with portions leased to private owners or owned by the State of Colorado. Somewhat less than 2,000 acres of the 7,500 acre study area are privately-owned, non-residential grazing lands. Quite a number of stock tanks, wells, impoundments and associated access roads are present across the area to support grazing use. Some recreational use of the National Grasslands is cited by the CSM.

Former Munitions Use. The study area includes two documented bombing targets (BT3 and BT4) and one suspected 75 mm air-to-ground target area inferred from an unsubstantiated record of the presence of a single 75 mm armor-piercing tracer round documented in the Archive Search Report (ASR) (USACE, 1995). The approximate locations of nine bombing targets were documented in the ASR, and the presence of an air-to-ground gunnery range plus submarine and ship skip bombing targets were documented but not located. Therefore, it was postulated prior to the demonstration that undocumented target locations could potentially lie within the study area.

Documented munitions present on the site surface within the study area includes AN-M30 and AN-M30-A1 General Purpose 100-lb bombs, M38A2 Mk15Mod3 100-lb practice bombs, 4 lb Incendiary Bombs, 50 caliber small arms rounds, and the single 75 mm AP cannon round. Air-to-ground rocketry by fighter squadrons stationed at La Junta Army Air Force (AAF) is documented in the ASR, however no documentation of the expected munitions type (possibly 2.25" practice or 5" high explosives [HE] rockets characteristic of the era) is provided in the findings.

3.4 Pre-Demonstration Testing and Analysis

Prior to data collection flights, a LiDAR calibration flight was completed over a known calibration site located at the Sky Research facility in Ashland, Oregon. This calibration flight served several purposes: to assess the alignment and offsets between the scanning mirror of the sensor, the IMU, and the GPS antenna on the aircraft; and to compare the results of the flight with known survey points. Assessing the alignment and offsets is necessary to ensure that flight lines will not be offset from one another. Comparing the calibration flight results with the known survey points allows for the calibration of the system to remove all possible offsets. The known survey points used for this comparison are 600 ground control points precisely surveyed on the Ashland airport runway and airport building corners.

The second part of the calibration flight included collecting high density LiDAR data over 30 simulated craters (Figure 4). These simulated craters range in depth from 5 centimeters (cm) to 40 cm and range in width from 0.25 meters (m) to 2 m (Figure 5). The data from the calibration

area were then processed and assessed to determine the minimal crater size that could be detected utilizing the LiDAR data.

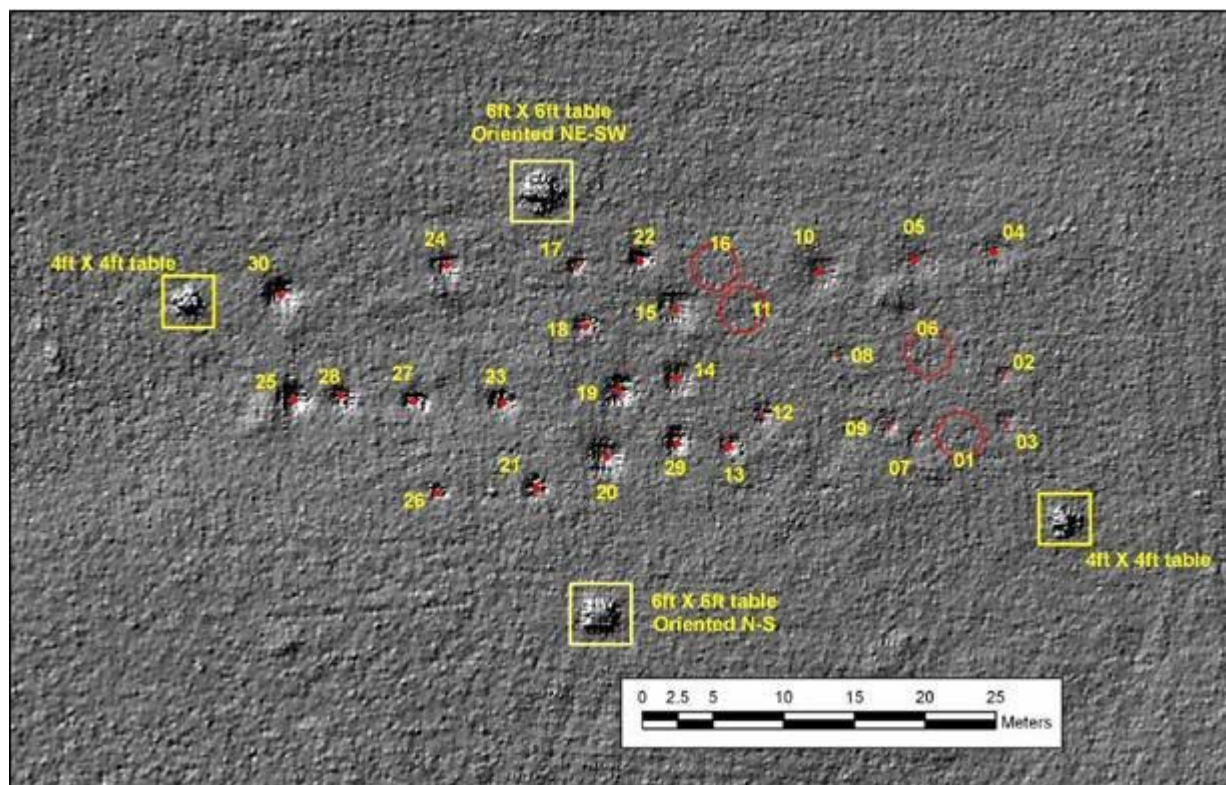


Figure 4. Crater calibration area at Sky Research calibration area in Ashland, Oregon.



Figure 5. Example of a calibration site crater with a diameter of 0.75 m and depth of 0.4 m.

3.5 Testing and Evaluation Plan

3.5.1. Demonstration Set-Up and Start-Up

Mobilization for this project required mobilization of the plane, equipment, pilot, and sensor operators from Ashland, Oregon, and deployment of ground support personnel to establish ground fiducials, establish and operate GPS base stations, and provide logistical support.

3.5.2. Crater Emplacement

Ten (i.e., “hand-dug”) craters were emplaced at the demonstration site for an assessment of crater detection ability. The emplaced craters consisted of a controlled series of circular depressions ranging from 45 to 177 cm in diameter and 11 to 30 cm in depth. The emplaced craters were located in the Phase II area north of BT3. In addition, 8 existing HE craters, ranging from 194 to 1,121 cm in diameter and 12 to 90 cm in depth were used for the crater detection analysis. Existing craters used in this analysis were a subset of craters originally identified in the Phase I demonstration area near BT4. The locations of all craters used in this analysis were recorded using RTK GPS measurements of the center point and a rim point.

To perform the assessment, both shaded relief and analytic images derived from the LiDAR bare earth elevation models were analyzed using crater analytical methods (described in Section 3.7.4). The shaded relief image was prepared using a light source azimuth of 315 degrees and an elevation of 45 degrees. The analytic image was prepared using a high-pass filter which subtracted the elevation value of each DEM cell from the mean of the surrounding neighborhood. The Phase I model had a resolution (DEM cell size) of 40 cm, and the Phase II model had a resolution of 50 cm. The ability to detect each crater using each type of imagery was classified into one of four categories, defined as follows:

- **HIGH:** Depression is detectable w/ automated and manual methods, and clearly circular/semi-circular.
- **MEDIUM:** Depression is detectable by manual visual inspection, but is difficult to separate from surrounding terrain.
- **LOW:** Depression is observable, but not diagnostic as a crater or distinguishable from natural terrain features.

- ND: Depression is not detectable.

3.5.3. Ground Control

A three-person ground support team operated GPS base stations, collected GPS road calibration transects, and placed ground control target panels for the LiDAR and orthophotography data collection. The ground support team included a professional land surveyor to ensure geospatial data accuracy, including maintaining accurate ties to the local coordinate system, and field emplacement of fiducials for data registration. RTK GPS technology was used for precision and efficiency in staking out survey grids and reference datums, in addition to other field positioning tasks.

Surface control was established at the site using ground fiducials of 4'x 4' plywood sheets raised 2' above the ground surface for LiDAR and 18" x 6' white plastic "X" aerial targets for orthophotography data collection (Figure 6). Ground fiducials for the LiDAR data collection were co-located with aerial targets for the orthophotography data collection, 1 per data collection tile (1 sq km). For the Phase I data collection, 9 LiDAR ground fiducials and 25 aerial targets were emplaced; for the Phase II data collection, 20 LiDAR ground fiducials and 30 aerial targets were emplaced (Figure 7). During all data collection flights, two dual frequency GPS base stations were collecting data at 1 second intervals.



Figure 6. LiDAR ground fiducial (left) and orthophotography aerial target (right).

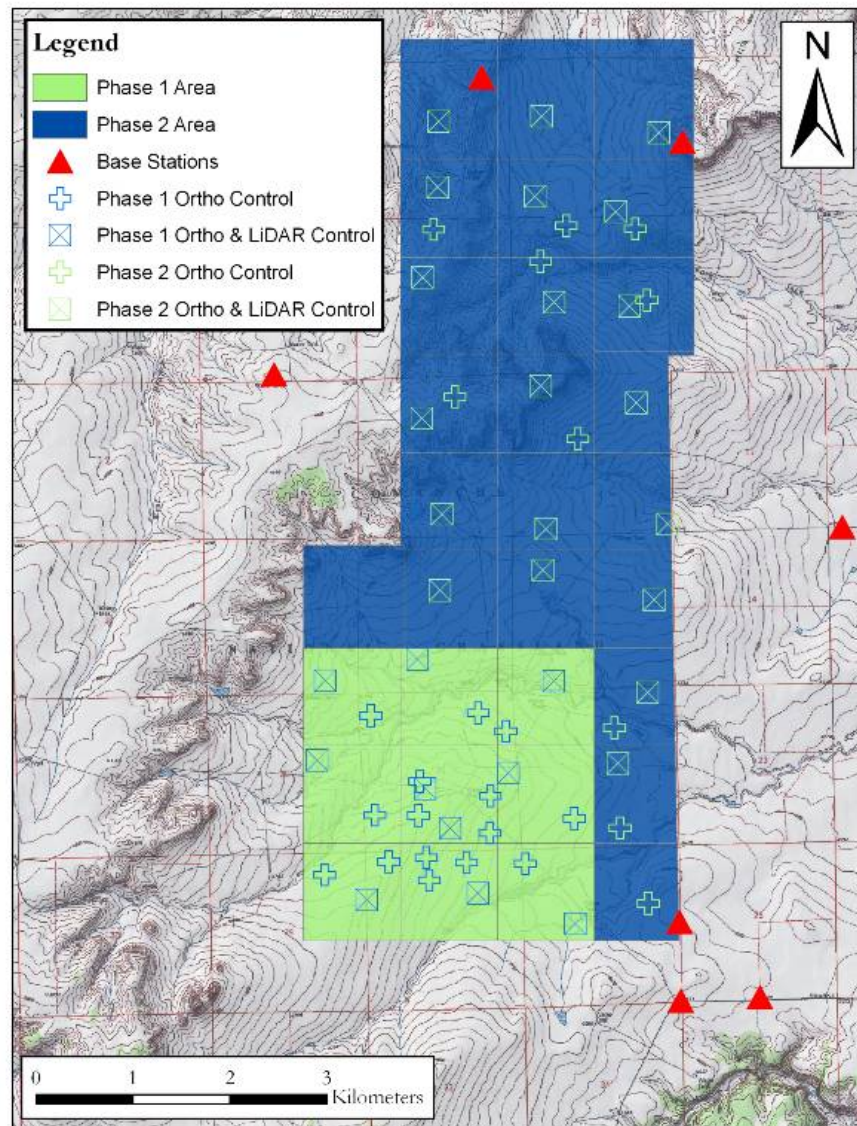


Figure 7. Ground fiducial emplacement for Phase I and Phase II data collection at Pueblo PBR#2.

3.5.4. Navigation Systems

An Applanix 510 A/V POS system was co-mounted with the LiDAR and orthophotography sensors to record the aircraft's GPS position utilizing a dual frequency GPS receiver and attitude (pitch, roll, and yaw) utilizing an IMU. The Optech ALTM-NAV software package was used for flight navigation. ALTM-NAV allowed the sensor operator to view in real time the swath of the laser system, images taken by the camera, PDOP levels, and number of satellites in the sky, as

well as any problems that could have occurred with the laser or camera system. The ALTM-NAV LED display mounted on the dash of the aircraft allowed the pilots to stay on each flight line within meters to ensure that data gaps did not occur.

3.5.5. Period of Operation

Phase I data collection occurred on August 20 and 23, 2004. Poor weather conditions prevented the data collection on either the 21st or 22nd. The data collection included the collection of both LiDAR data and orthophotography for approximately 6,700 acres of the Phase I study area. The two data collection flights took a total of approximately 5 hours to complete. Both data flights were completed between the hours of 10:30 am and 2:30 pm to ensure a good PDOP window, sufficient number of satellites, and sufficiently high sun angles (at least 30 degrees from the Earth's plane) for the photography.

Phase II data collection occurred on August 6, 2005. The data collection included the collection of both LiDAR data and orthophotography for approximately 6,600 acres of the PPBR#2 Phase II study area. The data collection flight took approximately 3.5 hours to complete and was completed between the hours of 10:30 am and 1:30 pm to ensure a good PDOP window, sufficient number of satellites, and sufficiently high sun angles for the photography.

3.5.6. Operating Parameters for the Technology

The flight parameters for Phase I and II LiDAR data acquisition were set to meet the required accuracies and spot spacings at the 800 m AGL flight altitude used for data collection. Flight-line spacing was approximately 230 m to allow a 50% overlap with the 560 m swath width achievable at 800 m. Table 5 summarizes the operating parameters for the LiDAR collection for the demonstration.

Orthophotography data were collected concurrently with the LiDAR data collection. Based on the LiDAR flight line spacing parameters, the orthophoto images were collected on every other LiDAR flight line, with a cross-track overlap of 36% and an along-track overlap of 30%. Table 6 summarizes the parameters for the orthophotography data collection for this demonstration.

Table 5. Acquisition Parameters for LiDAR Surveys at Pueblo PBR#2

Flight Altitude:	800 m AGL
Ground Speed:	105 knots
Measurements per second:	100,000
Scan Width:	370 m
Scan Overlap:	50% (185 m)
Scan Frequency:	60 Hz
Scan Angle:	+/- 13
Spot Spacing:	0.44 m

Table 6. Color Orthophotography Data Acquisition Parameters

Field of View:	36°
Imaging Swath/Photo Coverage:	36% cross-track overlap; 30% along-track overlap
Ortho-rectified Pixel Size, Re-sampled	0.16 m/pixel

For the Phase I orthophotography data collection, the 6,600 acre study area was buffered substantially by 1.5 km (Figure 8). This was necessary to collect and process enough photography to ensure that all the extents of the project area contain adequate amounts of tie points. The data collection resulted in a total of 858 photos, of which approximately 400 were then used in data processing.

As in the Phase I data collection, the Phase II data collection study area was also substantially buffered (Figure 9). The data collection resulted in a total of 721 photos, of which approximately 650 were then used in data processing.

3.5.7. Demobilization

At the conclusion of the surveys, the aircraft, associated equipment, and field crews were demobilized from the site.

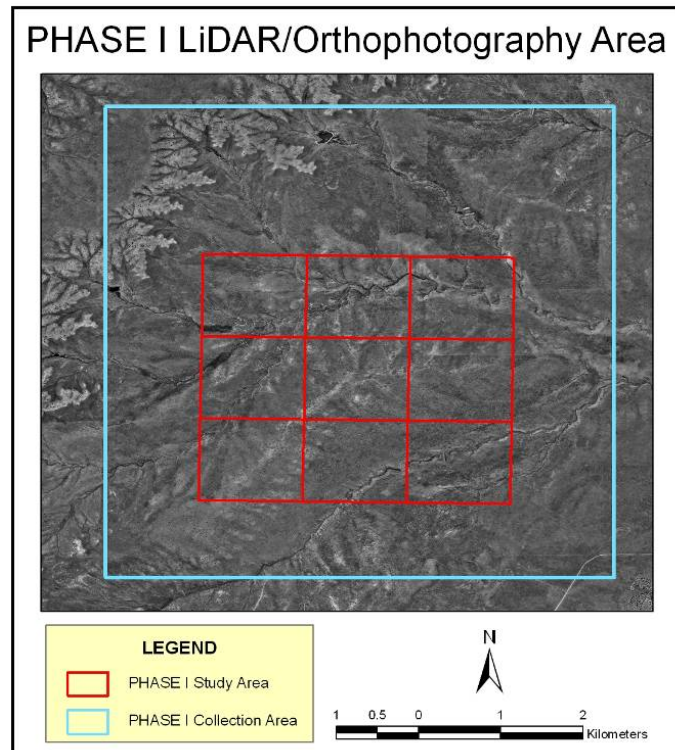


Figure 8. Phase I orthophotography data collection boundaries.

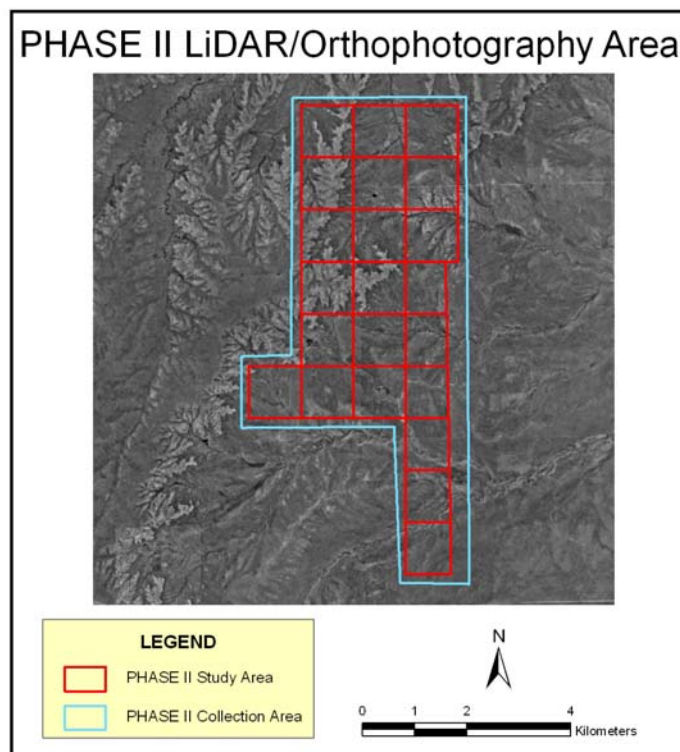


Figure 9. Phase II orthophotography data collection boundaries.

3.6. Data Processing

3.6.1. LiDAR Data Processing

LiDAR processing transforms raw binary data into a functional DEM. LiDAR processing was conducted in the following seven steps:

1. **GPS post-processing:** Post-processing of GPS datasets was completed using POSpac/POSGPS® software. Multiple baseline solutions were combined to determine the x,y,z position of the aircraft within 4 inches.
2. **IMU/GPS SBET processing:** The post-processed GPS data were then combined with the IMU data using a processing technique commonly referred to as smoothed best estimate trajectory (SBET) processing. This method combined information about orientation and velocity from the IMU with positioning and velocity information from the GPS data using Kalman filters (the Kalman filter is a data processing algorithm that minimizes mean squared error). The result was a determination of the x,y,z and ω, κ, ϕ parameters for the aircraft at any particular point (position in Universal Transverse Mercator [UTM] 1983 North American Datum [NAD83] meters and the angular orientation of the aircraft). This processing was performed in the proprietary software, POSProc.
3. **LiDAR raw data extraction:** The raw LiDAR data were copied from tape and extracted from the raw data acquisition format into a pre-processed format for output into x,y,z points. Information from the sensor calibration was input into the processing at this point.
4. **LiDAR data calibration:** The variations in altitude and temperatures encountered during normal aircraft operations change the physical characteristics of the LiDAR optics to such a degree that corrections are required. These corrections were completed using manual data calibration techniques created in-house by Sky Research.
5. **LiDAR data output:** Pre-processed LiDAR data were combined with the SBET IMU/GPS data to form the final x,y,z data cloud. This data cloud included all of the returns collected during data acquisition, with each return having an exact x,y,z location.

6. **LiDAR classification:** The x,y,z data cloud was imported into TerraScan LiDAR processing software. Next, the data was classified into point classes. First, all points that were beyond the known elevations of the survey area (known as error points) were removed. The remaining points were then classified automatically and manually into two separate classes: 1) points that represent the ground surface; and 2) all other points that are above the ground surface.

3.6.2. Orthophotography Data Processing

Primary processing of raw digital camera data resulted in a seamless, orthometrically correct 24-bit red-green-blue (RGB) aerial photomap of the site. This true-color imagery was collected and processed to resolve landscape features less than 1 foot across. Sky Research processed orthophotography data in the following steps:

1. **Photo development:** Raw photos were developed into TIFF format with a manufacturer-calibrated true-color (VIS) filter.
2. **GPS post-processing:** Post processing of GPS datasets was performed using POSpac/POSGPS® software. Multiple baseline solutions were combined to determine the x,y,z position of the aircraft within 4 inches.
3. **IMU/GPS SBET processing:** The post-processed GPS data were then combined with the IMU data using SBET. This method combines information about orientation and velocity from the IMU with positioning and velocity information from the GPS data using Kalman filters. The result was a determination of the x, y, z and ω, κ, ϕ parameters for the aircraft at any particular point (position in UTM NAD83 meters and the angular orientation of the aircraft). Also extracted from this process was an event file documenting the GPS time and POS event identification (ID) for each photograph exposure. This processing was performed in the proprietary software, POSProc.
4. **Camera Photograph ID extraction:** A camera-specific event file was extracted from Camera Mission Folder using DSS Mission View 2.0, containing GPS time and camera photograph ID.
5. **Exterior orientation extraction:** POS photograph event ID and camera photograph ID documents were synced by GPS time and processed in POSEO 4.1. This process

incorporated the SBET file with event IDs to create an exterior orientation file assigning x and y center point locations, pitch, roll, and heading to each photograph.

6. **Auto triangulation:** Formatted image files were combined with the exterior orientation file in ISAT software (Figure 10). Tie points were generated automatically using intensity values within designated von Gruber (an automated method for determining tie points within an image) areas. Thirty-six von Gruber areas were assigned per photograph, and approximately eight tie points were generated per von Gruber area. The RMSE for each tie point was calculated using survey control. RMSE and residuals were calculated for all photographs using survey control. Solution for triangulation is accepted when RMSE was less than 1/10,000th of the flying height and residual was less than 1/5,000th of the flying height. Each photo was then adjusted according to individual triangulation results as well as adjusted to the entire data set.
7. **Orthophoto creation:** Triangulation results were loaded into ortho-processing software, along with a LiDAR-derived DTM and aerial photography. Aerial photographs were rectified to the DTM using ImageStation Ortho Pro software. Seam lines were automatically generated based on photo centers then edited for feature consistency. These seam lines designate the point at which multiple photos are to be spliced to form a single mosaic tile (Figure 11). The ortho-corrected photography was then mosaiced into tiles and stored in a geodatabase as a seamless raster.

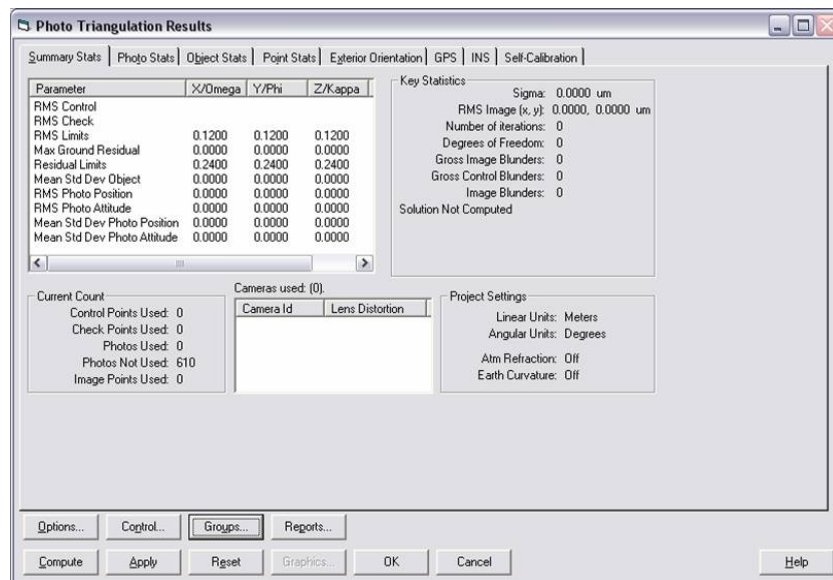


Figure 10. Screenshot of ISAT aerotriangulation results window.

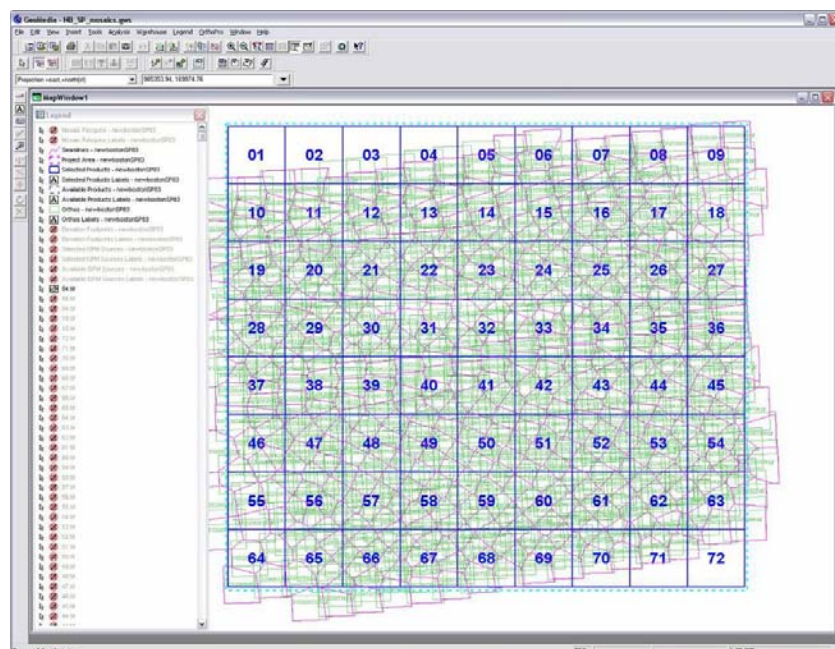


Figure 11. Screenshot of OrthoPro seam lines (pink), tiles (blue), and photos (green).

The total size of raw photo data collected amounted to approximately 13.9 gigabytes (GB) for Phase I data and 23.7 GB for Phase II data. This number represents the total number of compressed images as well as navigation data necessary for external orientation processing.

3.7. Data Analysis

Secondary analyses included conversion of processed sensor datasets into suspected munitions-related feature datasets utilizing a variety of processing and analytical techniques. These analyses resulted in feature mapping information from sensor data describing the character and location of probable UXO contamination on the site that could be directly related to historical use data for the site. Detected features were stored in the dataset FEATURE_OF_INTEREST_CSMV1.

Several image processing steps were used to generate derivative raster datasets that enhance feature detection, followed by a systematic manual inspection and interpretation of the imagery in a GIS workstation environment that facilitates multiple image overlays with transparency and edge-sweep controls, contrast stretching, multiple-band blending in an RGB color model and

other visualization tools, together with the ability to extract interpreted image features into vector point and polygon map features in the geodatabase. The following is a discussion of the data analytical procedures followed for interpretation of LiDAR and orthophotography datasets.

3.7.1. Computation of Derivative LiDAR Images

The LiDAR bare earth DEM is used to compute two different derivative images including a “hillshade” image and an “analytic” image. The hillshade was computed using a raster analysis function that computes the hypothetical illumination of a surface by determining illumination values on a cell-by-cell basis for each cell in the image. This was accomplished by defining a vector for a hypothetical light source (azimuth and elevation) and calculating the illumination value for each cell in relation to neighboring cells. A hillshade image was computed for the entire site using a standard az=315/elev=45 source vector and saved to the geodatabase for performance and consistency, and the operator varied these parameters (and others such as vertical exaggeration) as required to enhance feature visualization. The second derivative “analytic” image was a high-pass filter of the bare earth DEM computed by subtracting the elevation value of each DEM cell from the average of the surrounding cells in a defined circular neighborhood. This process resulted in an image that emphasizes micro-topographic features in the image of a scale correlated with the filter’s search radius. The neighborhood radius was revised as needed by the operator to enhance visualization of features of various size and shape.

3.7.2. Image Analysis Grids

To enable an efficient and systematic analysis, the study area was subdivided into 100 m grid cells, and each 100 m cell was further subdivided into 20 m cells. This two-tiered grid system was used by the operator to track progress and ensure complete and even review of the imagery as multiple images were overlaid, and examined at various scales and combinations. These analysis grids were quickly generated in ESRI shape file format using standard GIS tools.

3.7.3. Target Feature Identification and Extraction

ESRI ArcGIS Desktop client software environment, the standard operator environment for visualizing, identifying and extracting anthropogenic landscape features qualifying as potential target features, provided visualization tools for revealing and registering underlying image layers, and draping images on the DEM for three dimensional (3D) rendering, for visualization and interpretation of the data. Available datasets within each grid cell were systematically

examined for target features including circles, “cross-hair” aiming points, ship outlines, and rectangular shapes that could represent airstrips, buildings, or other target types. As features were identified in an image and corroborated in other imagery, outlines were digitized by the operator into a feature-class geodatabase layer and assigned attributes such as area, centroid, primary and corroborating sensors, description, and feature type, calculated by the remote sensing analyst. Extracted target features were stored in the “Area of Interest” feature class in the geodatabase (Appendix C).

3.7.4. Crater Feature Identification and Extraction

Crater feature identification and extraction utilized the LiDAR-derived hillshade and analytic high-pass DEM images. For purposes of a crater detection analysis, high explosive (HE) impact craters were defined as circular or semi-circular depressions of any size up to 20 m in diameter. Perimeter circularity, concave bottom profile and raised rim were considered to be diagnostic attributes. To classify a depression as a crater, any significant irregularity of shape (departure from circularity) should be explained by adjacent crater features, rock outcrops, or recent disturbance.

As with target feature extraction, the datasets were analyzed using a systematic manual inspection and interpretation of the imagery in a GIS workstation environment. An automated circular depression detection algorithm was also applied for detecting craters. The automated detection was used to generate candidate detections that were verified or rejected in the manual extraction.

3.7.4.1. Automated Crater Detection

For automated crater detection, the Feature Analyst extension for ArcGIS was used with a custom radial search pattern to generate a preliminary set of topographic depression detections across the study area. Training polygons were established on a variety of obvious crater features identified in the shaded relief imagery, ranging in size from 4 m to 20 m. Four meters were used as the minimum training polygon to minimize the large number of false-detections generated by smaller training shapes. A custom radial search pattern was designed for use by the Feature Analyst spatial classifier that optimized detection of crater-like depressions. The classifier was run directly on the bare earth DEM raster. Once the preliminary depression detections were converted to a polygon GIS feature class, a circularity shape factor was computed for each polygon ($4 * \pi * \text{Area} / (\text{perimeter}^2)$). This shape factor was a type of area/perimeter ratio that results in 1 for a perfect circle and gets smaller as the shape departs from a circle. The circularity

attribute was used in the manual extraction of crater features.

3.7.4.2. Manual Crater Extraction

Using the processing grids described above, the operator visually identified each crater in a grid sector and digitized a circular feature centered on the center of the crater with the perimeter set to a radius that best follows the rim of the identified crater. Overlapping craters were digitized as overlapping circles. The operator used the LiDAR shaded relief and analytic high-pass DEM imagery as the basic visualization cue, while the orthophotography was used to support the manual identification by observing vegetation features that respond to altered surface hydrology. The operator used the automated classification image by setting the circularity threshold and observing the locations of auto-detected depressions to check for any features that may have been missed manually. After the craters were digitized for each analysis grid, the operator ran a custom spatial analysis script within the ArcGIS environment that extracted the high and low elevations within each circle from the underlying DEM, and stored these elevations and the difference (crater depth) as attributes for each. Crater area, perimeter length, and centroid coordinates were also saved as feature attributes. The resulting polygon feature class was saved in the project geodatabase (Appendix C).

3.7.4.3. Crater Density Analysis

To visualize the distribution of craters across the study area, a density analysis was performed by computing a kernel density raster whose cell values each describe the crater density in craters per hectare of a circular neighborhood around each cell. Changes in the neighborhood radius affect the resulting density surface, with larger radii producing a more generalized density model and smaller radii producing more detail. Therefore, a neighborhood radius appropriate to the crater density and patterns was interactively determined to produce a density surface most appropriate to the distribution of craters across the study area landscape.

3.7.5. Range Infrastructure Identification and Extraction

The LiDAR and orthophoto datasets were analyzed to extract other anthropogenic features that can aid interpretation and characterization of the UXO contamination patterns on the site by the spatial correlation of extracted features such as transport routes and evidence of excavation activities with documentary site usage information.

The feature extraction methodology used to extract infrastructure features was essentially the same as that described for the identification and extraction of target features and is conducted concurrently with that extraction. These features were incorporated into the CSM Feature of Interest and Corridors feature classes in the geodatabase and include observed vehicle routes across the study area and locations where the datasets indicate excavation or other grading, fences, utilities, structures, and foundation pads.

4. Performance Assessment

4.1 Crater Detection Analysis

Table 7 presents the results of the crater detection assessment performed at the demonstration site as described in Section 3.5.2. The reported results includes the detection classification (i.e., High, Medium, Low, ND) for both the LiDAR derived hillshade and analytic high pass imagery types and the estimated diameter and depth. Crater diameter was computed by constructing a circular polygon feature centered on the surveyed center point with the circumference passing through the corresponding rim point. Crater depth was computed from the elevation difference between the center point and the rim point.

Table 7. Diagnostic Detectability of Crater Features in LiDAR Imagery

Crater ID	Hillshade	Analytic	Diameter (cm)	Depth (cm)
17	High	High	1121	90
15	High	High	564	50
16	High	High	534	37
19	High	High	501	36
13	High	High	399	31
14	Medium	High	353	24
20	Low	Medium	288	14
18	Low	Medium	194	12
1	Low	Medium	177	30
3	Low	Low	166	30
7	ND	Low	104	28
12	ND	ND	74	13
2	ND	ND	74	11
10	ND	ND	65	24
5	ND	ND	63	25
11	ND	ND	54	28
9	ND	ND	46	20
8	ND	ND	45	20

These results illustrate that the detectability threshold for HE craters in the 40-50 cm resolution LiDAR ground model is a diameter of about 150 cm (approximately 9 pixels), and the diagnostic threshold (terrain depression can be recognized as a probable HE crater) is a depression diameter

of about 350 cm (approximately 50 pixels). The difference in image type response at the diagnostic threshold results from the improved detectability of the characteristic raised “berm” of excavated soil around the perimeter of the “real” craters, and the improved contrast of even small circular depressions with surrounding terrain. Figures 12 through 15 show the 18 assessment craters on both hillshade and analytic high-pass imagery.

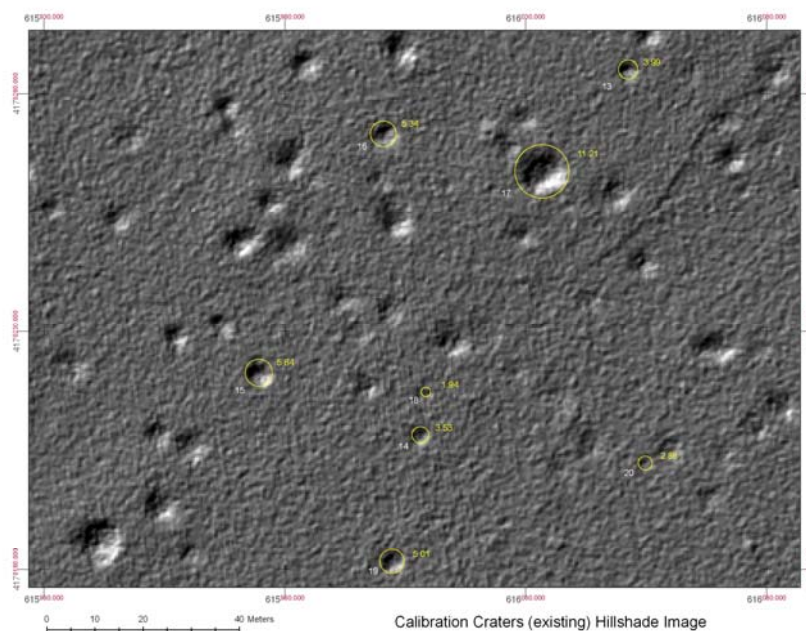


Figure 12. Calibration craters (existing), hillshade image.

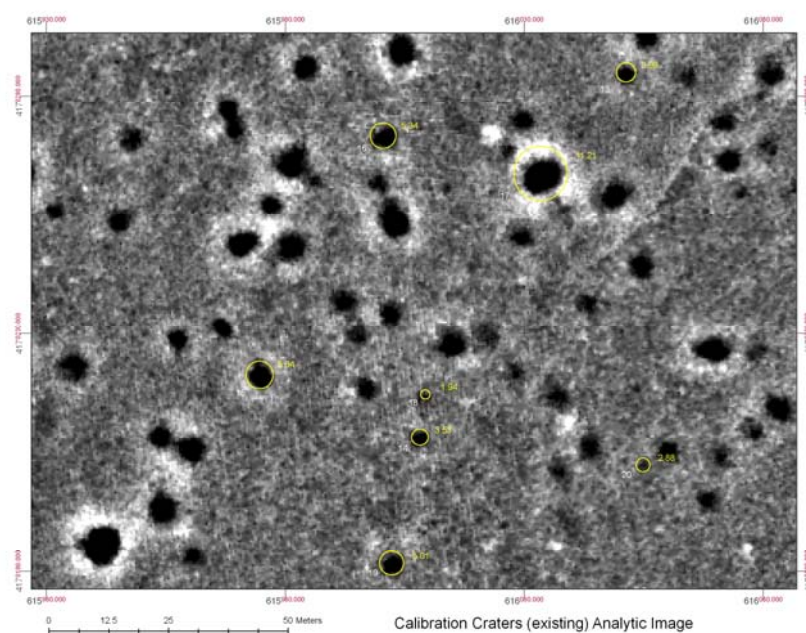


Figure 13. Calibration craters (existing), analytic image.

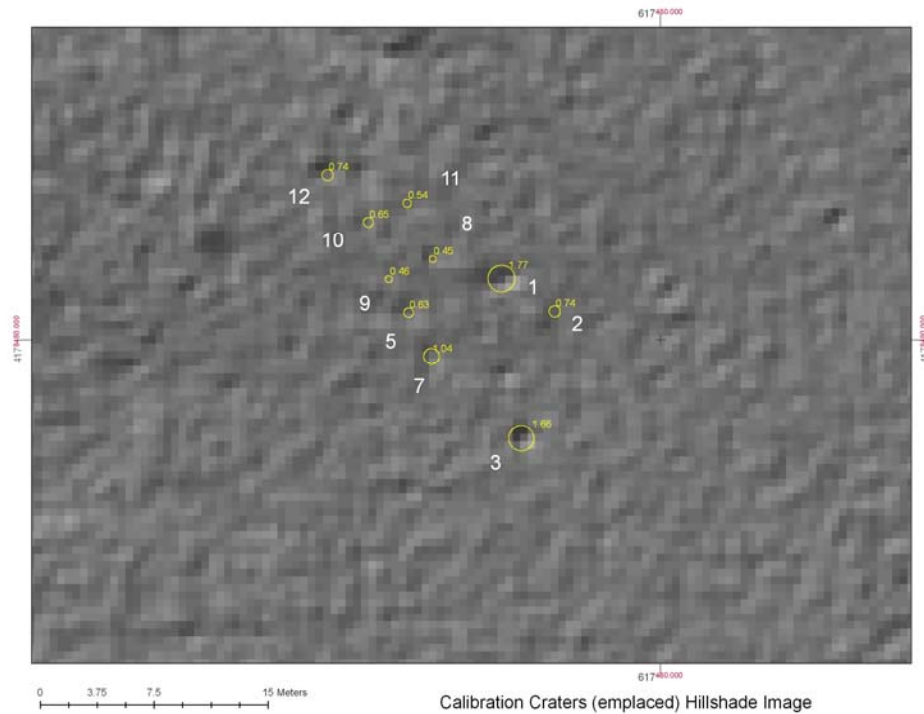


Figure 14. Calibration craters (emplaced), hillshade image.

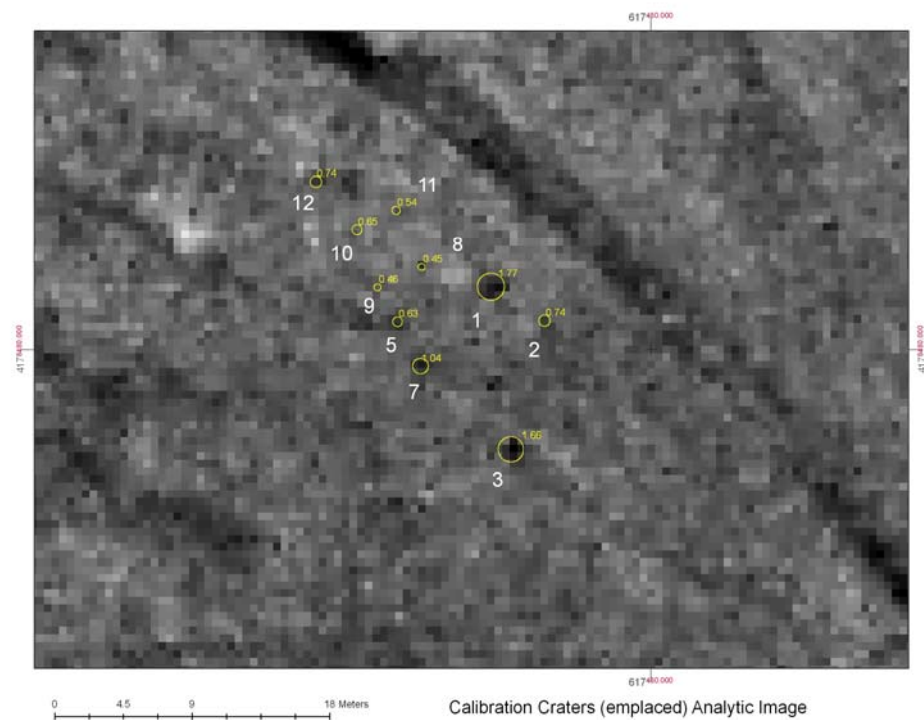


Figure 15. Calibration craters (emplaced), analytic image.

4.2 Spatial Accuracy

4.2.1 LiDAR Data Spatial Accuracy

To determine spatial accuracy, horizontal offsets were calculated by determining the centroid of the modeled perimeter versus surveyed center point. Vertical offsets were calculated from average feature surface elevation versus surveyed center point elevation (Figure 16). Spatial accuracy for the LiDAR data collection achieved the goals for the project as shown in Table 8.

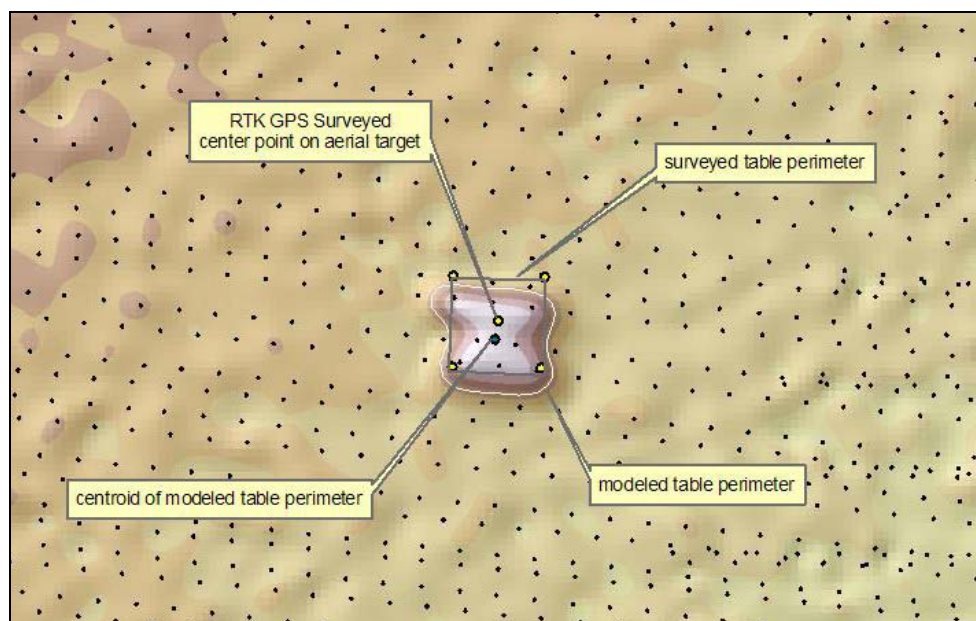


Figure 16. LiDAR spatial accuracy assessment methodology.

Table 8. LiDAR Data Accuracy Results

Accuracy Metrics	Phase I Data (m)	Phase II data (m)
Y RMSE	0.070	0.092
Y Linear Error (95% confidence level)	0.137	0.181
X RMSE	0.274	0.076
X Linear Error (95% confidence level)	0.537	0.152
RMSE Horizontal Radial Error (68.3% confidence level)	0.282	0.085
Horizontal Radial Error (95% confidence level)	0.421	0.166
RMSE Vertical Linear Error (68.3% confidence level)	0.111	0.032
Vertical Linear Error (95% confidence level)	0.218	0.063

4.2.2 Orthophotography Data Spatial Accuracy

To determine orthophotography spatial accuracy, image coordinates of ground targets were compared to GPS position, and X-Y offsets were calculated (Figure 17). Spatial accuracy for the orthophotography data collection achieved the goals for the project as shown in Table 9.

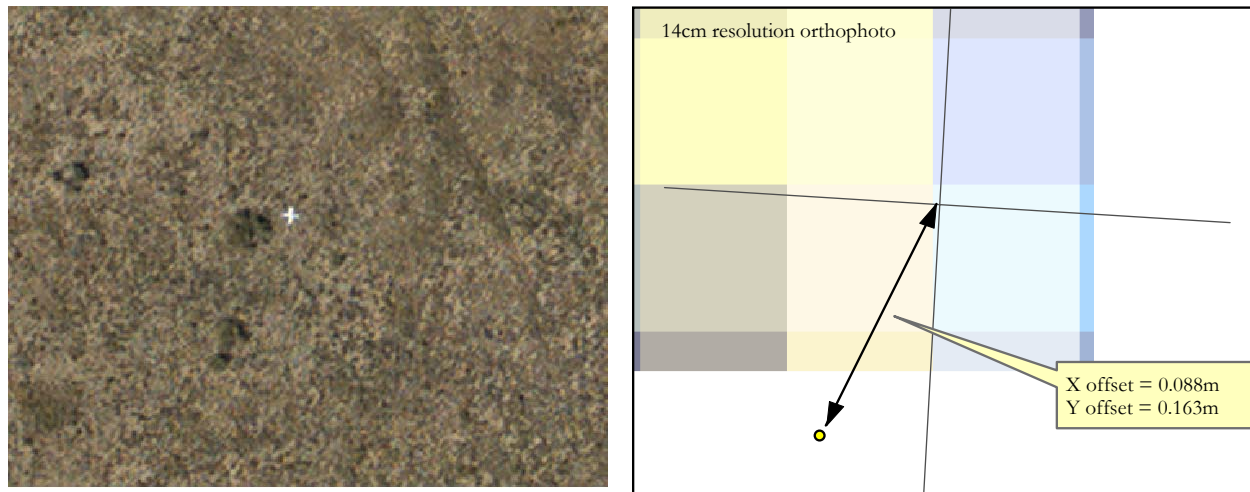


Figure 17. Orthophotography spatial accuracy assessment methodology.

Table 9. Orthophotography Data Accuracy Results

Accuracy Metrics	Phase I Data (m)	Phase II data (m)
Y RMSE	0.131	0.099
Y Linear Error (95% confidence level)	0.257	0.195
X RMSE	0.103	0.120
X Linear Error (95% confidence level)	0.202	0.235
RMSE Horizontal Radial Error (68.3% confidence level)	0.286	0.268
Horizontal Radial Error (95% confidence level)	0.562	0.526

4.3 Data Analysis Results

4.3.1 Target Area Detection

Target features anticipated to be present on the study area site based on historical data in the CSM Version 0, (Versar, 2005) included target circles at bombing BT3 and BT4 observed in the

1951 aerial photography. The 1995 ASR field inspections located the aiming circle at BT3, but did not observe other target features (other potential HE craters). The 1995 ASR mentions the construction of an Air-Ground Gunnery Range, conversion of 5 of the 9 precision bombing targets to E-1 Sonic Scoring targets, and the construction of skip bombing (ship) and submarine targets several years after the range was initially put into operation. Locations for these upgraded targets were not documented.

Determination of the presence, characteristics, and exact location of target features within the study area relied on the use of high resolution optical remote sensing datasets including LiDAR, large-scale color orthophotography, and the hyperspectral imaging (HSI) (Sky Research, 2007) datasets. The bombing targets at Pueblo PBR#2 were constructed from earthen berms or flat-graded/depressed paint strips, generating micro-topographic features observable in the high resolution LiDAR ground model DEM. Vegetation characteristic of disturbance and eroded topsoil is also associated with these features, observable in the high resolution orthophotography. Patterns of vegetation and soil disturbance, and (potentially) remnant marking paint or herbicides are also observable in the coarser resolution HSI data (Sky Research, 2007).

These datasets were georeferenced with known geographic accuracy, and co-registered so that the location of extracted features could be established in the field using RTK GPS technology. The combined results of the target feature analysis for Phase I and Phase II, including the documented locations for BT3, BT4, and the 75 mm Suspected Target, are included in the “Area of Interest” geodatabase feature class (Appendix C).

4.3.1.1 BT3

In the documented BT3 area, target features were best-defined in the LiDAR analytic image and corroborated in all the other image datasets (Figure 18). The aiming circle was delineated, with a diameter of 320 m, and inner concentric circles identified, a 180 m x 115 m raised area within the aiming circle to the east, and a fenced area extending outside the aiming circle to the west (Figure 19). No crosshair features (as mapped for BT4) were mapped, even though some evidence for northern and western crosshair arms is suggested in the data. A possible ship target was partially detected west of the aiming circle (Figure 20). An area north of the aiming circle,

approximately 100 m x 100 m, was identified as being a possible feature of interest related to BT3; this feature is comprised of raised areas indicative of potential berm-like features (Figure 20). Much of the BT3 area was disturbed by more recent erosion-control grading consisting of 50 or more small earthen check-dams constructed across erosion features, many of which appear to have originated from the target circle and access road grading for the target.

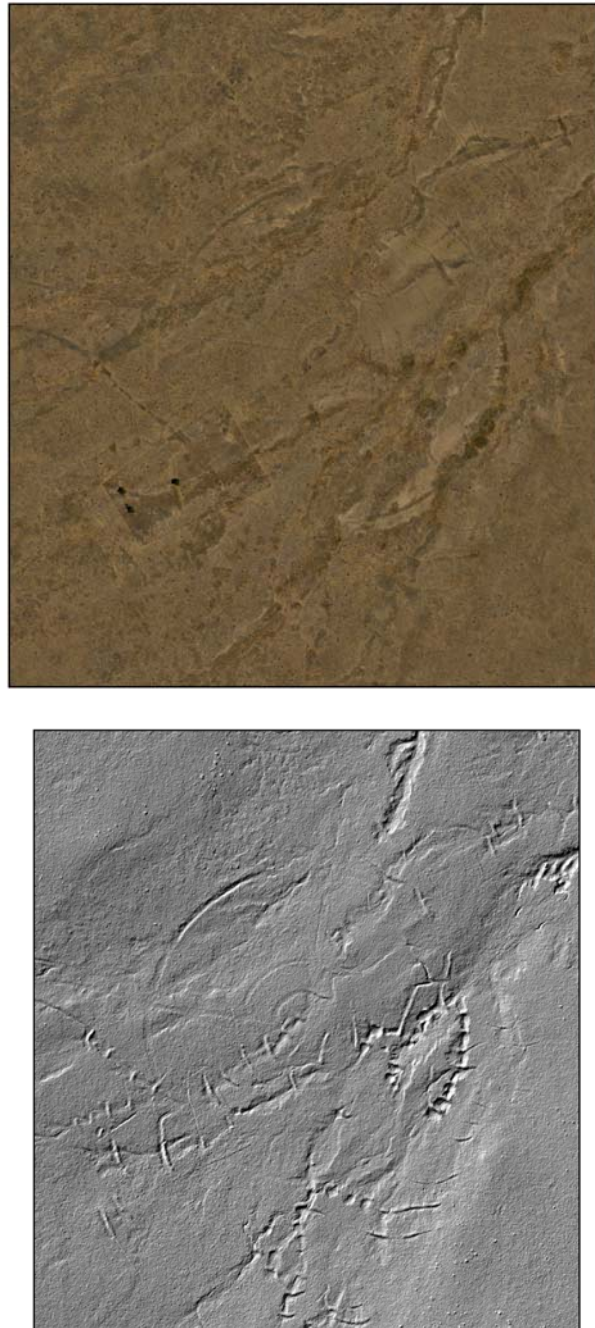


Figure 18. BT3 target circle as detected in orthophotography (top) and LiDAR (bottom) imagery.

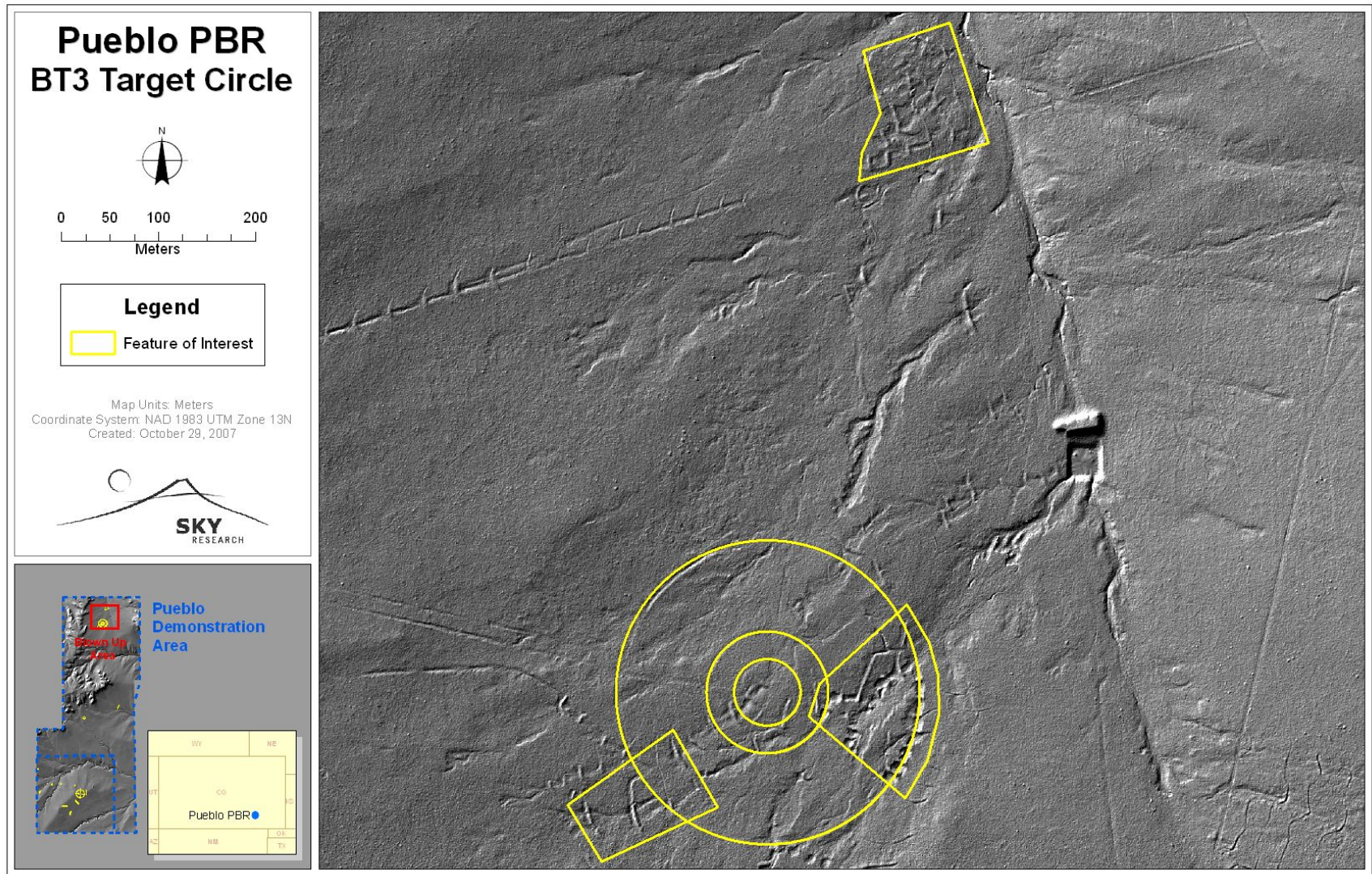


Figure 19. Delineation of target features at BT3 and vicinity.

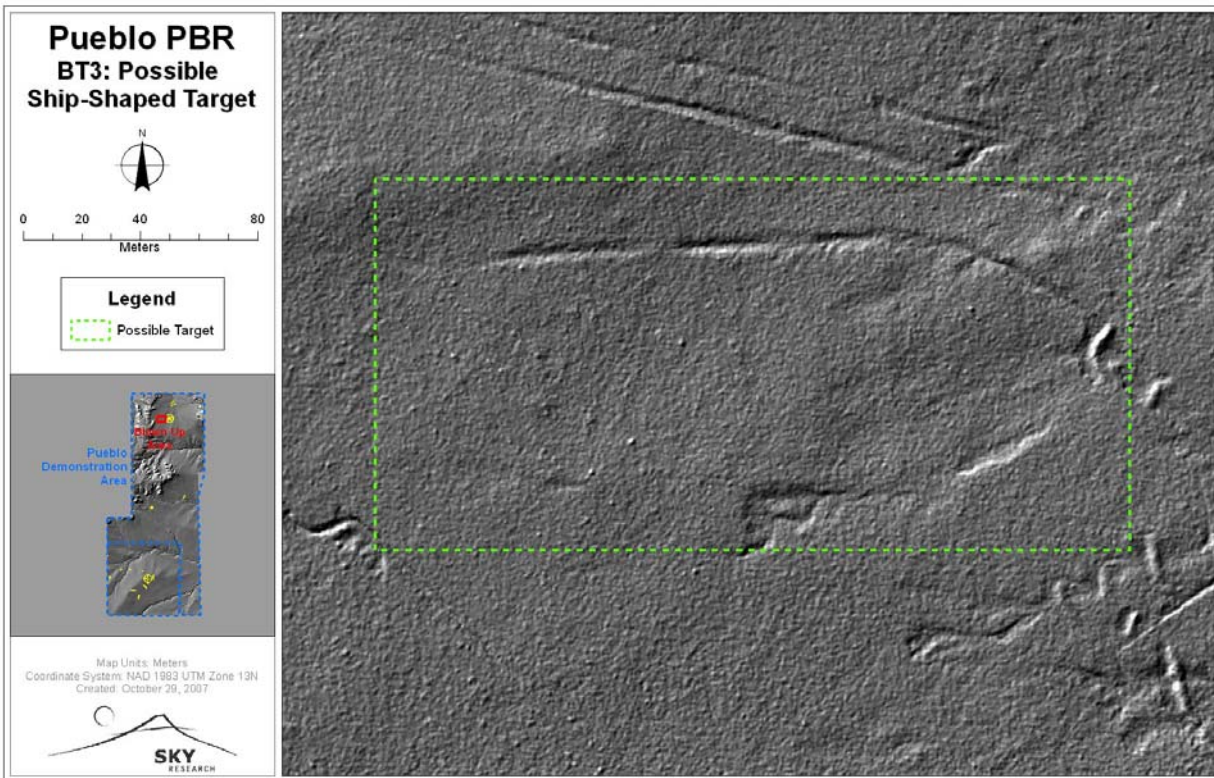


Figure 20. Partial ship outline at BT3, located on the western side of aiming circle.

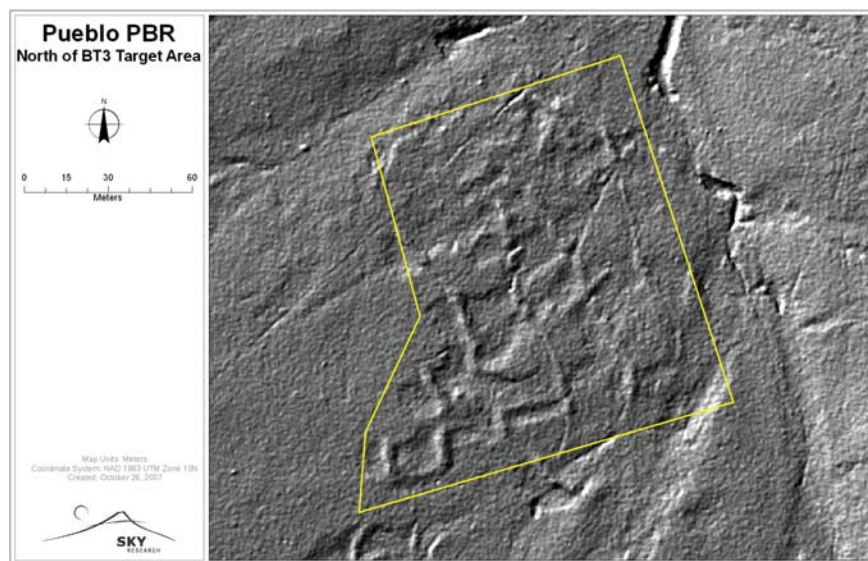


Figure 21. Raised features identified north of BT3 target circle.

4.3.1.2 BT4

In the documented BT4 area, a 1,000 foot in diameter aiming circle was mapped; the aiming circle was intersected by a four-armed crosshair oriented NS-EW, each arm extending from the inner 200' circle to about 100' past the outer circle (Figure 21). These features were constructed by flat-grading the pattern in lines approximately 5 m wide, resulting in minor (generally less than 0.5 m below adjacent surfaces) circular and linear depressions.

Four ship targets ranging in length from about 160 to 210 m were mapped in the vicinity of BT4 (Figure 22). These features were constructed by grading raised berms in the shape of ship outlines, representing in approximate size and shape a WWII-era Japanese or German battleship. It is postulated that these target features at least partially account for the skip targets described in the ASR. These features are also best defined in the analytic high-pass LiDAR image (Figure 23). One ship target (immediately SSW of the BT4 circle) is observable in the HSI false-color minimum noise fraction (MNF) and high-pass LiDAR DEM imagery, but not in the orthophotography or hillshade images analyzed in the work (Figure 24).

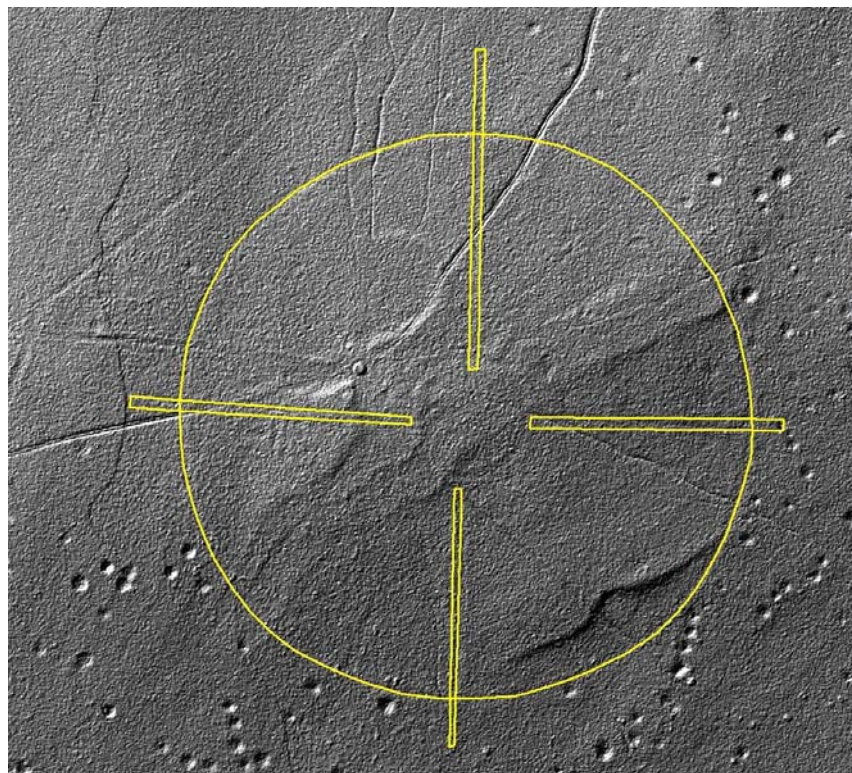


Figure 22. BT4 aiming circle with crosshairs delineated.

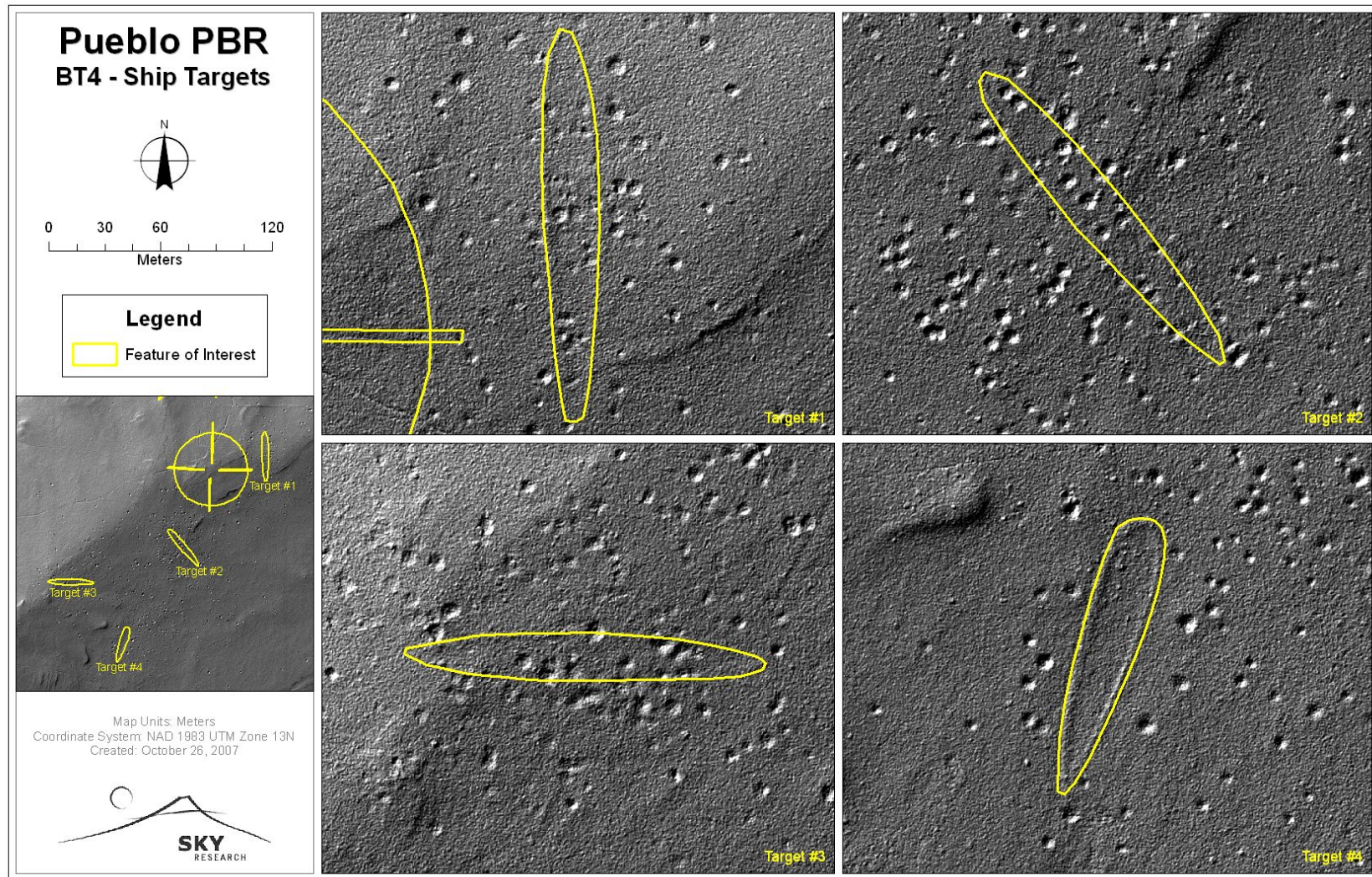


Figure 23. Four ship targets were detected in the LiDAR imagery in the vicinity of BT4.

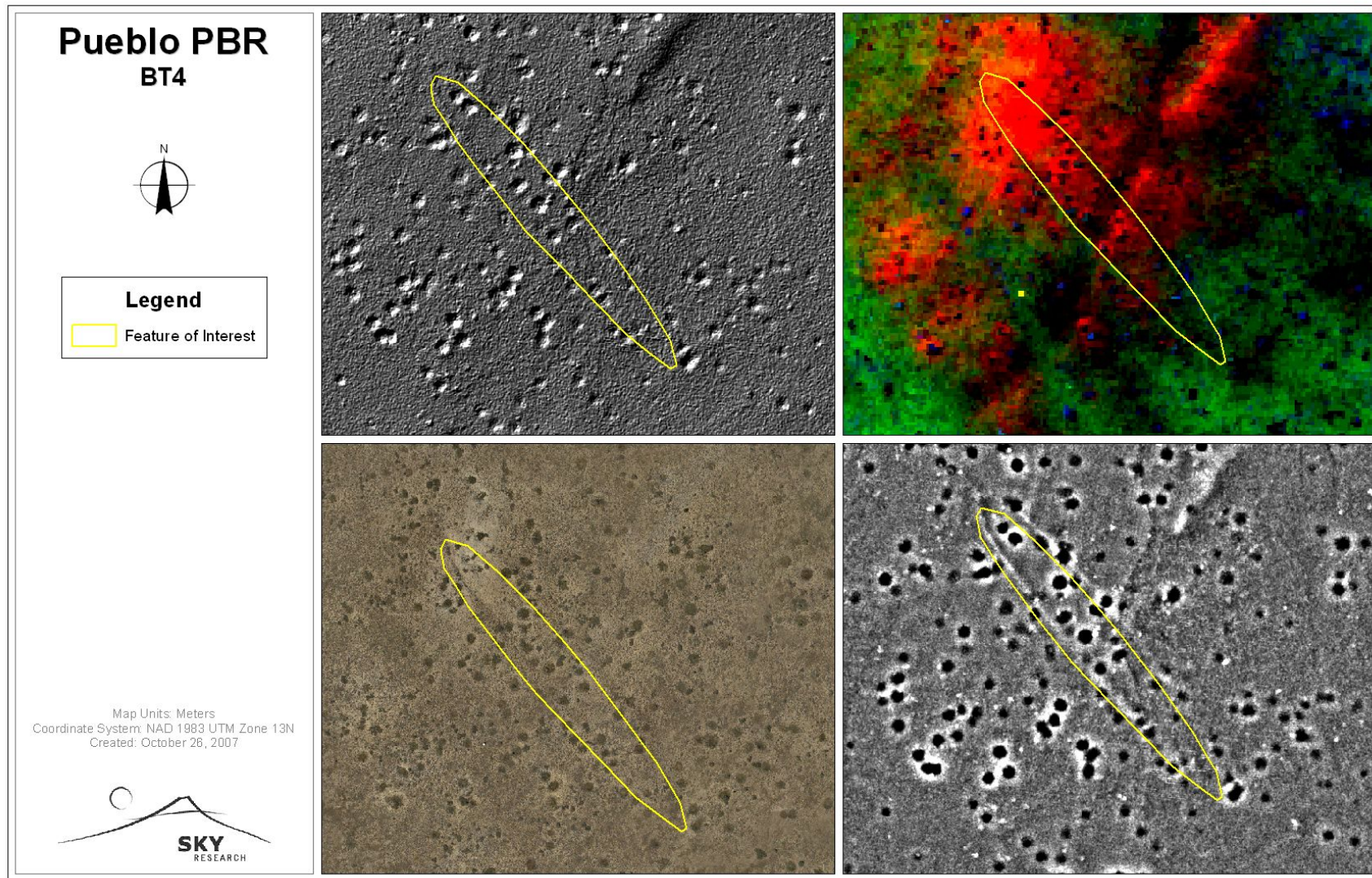


Figure 24. Ship target at BT4 feature as overlain on LiDAR hillshade (top left); HSI (top right), orthophotography (bottom left) and LiDAR high-pass (bottom right) imagery.

4.3.1.3 75 mm Suspected Target

No munitions related features were detected in the vicinity of the suspected 75 mm target in either the orthophotography or the LiDAR imagery (Figure 25).

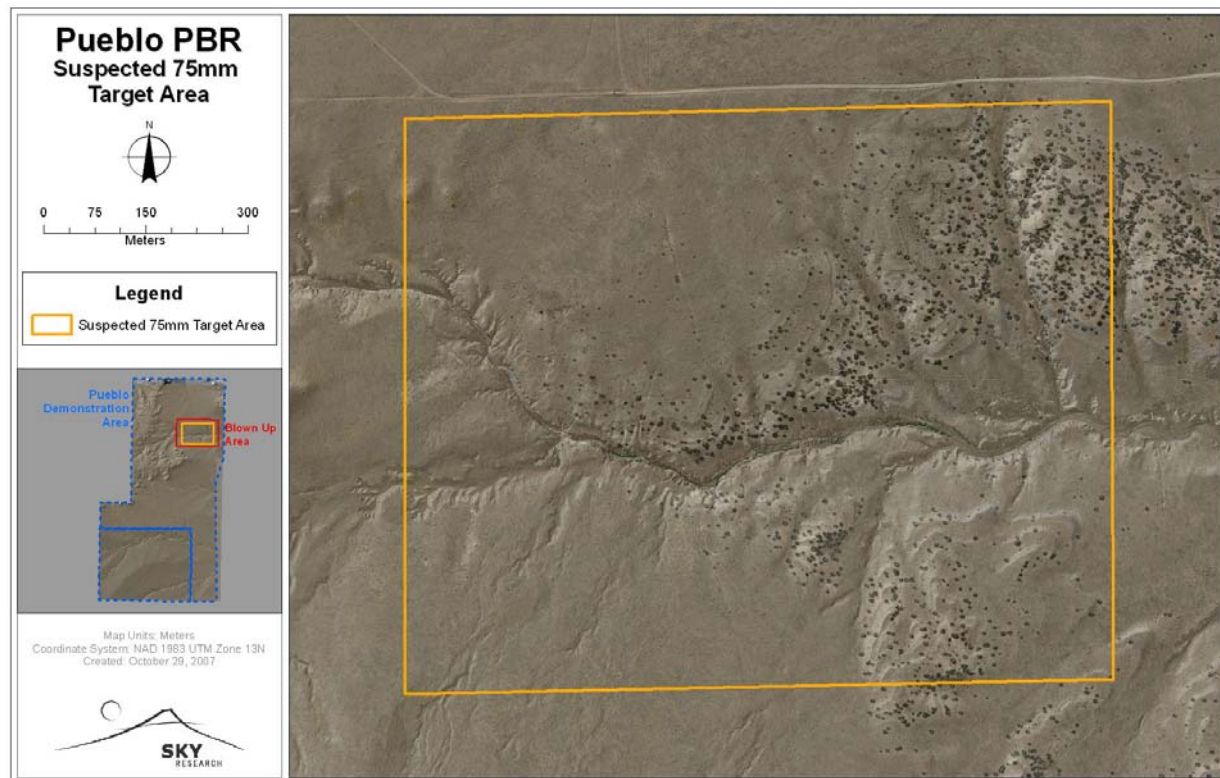


Figure 25. No munitions related features were detected within the boundaries of the Suspected 75 mm Target Area (1995 ASR boundaries).

4.3.2 Crater Detection

A total of 1,103 potential crater features were mapped on the combined Phase I and Phase II study areas. The crater-like features detected using the LiDAR imagery ranged in diameter from 200 cm to about 1,500 cm, with an average of about 800 cm, and ranged in depth from 13 cm to 148 cm, averaging 51 cm in depth. Density analyses of the crater-like features were performed using a neighborhood radius of 75 m to produce a density surface appropriate for the distribution of craters across the Pueblo demonstration site. The combined results of the potential crater feature analysis for Phase I and Phase II, including the polygon feature class that stores the size

and location of each identified crater-like feature and its attributes and the density summary datasets, are included in the geodatabase.

4.3.2.1 BT3

Sixteen potential craters were mapped in the vicinity of BT3; half of these were outside the aiming circle (Figure 26).

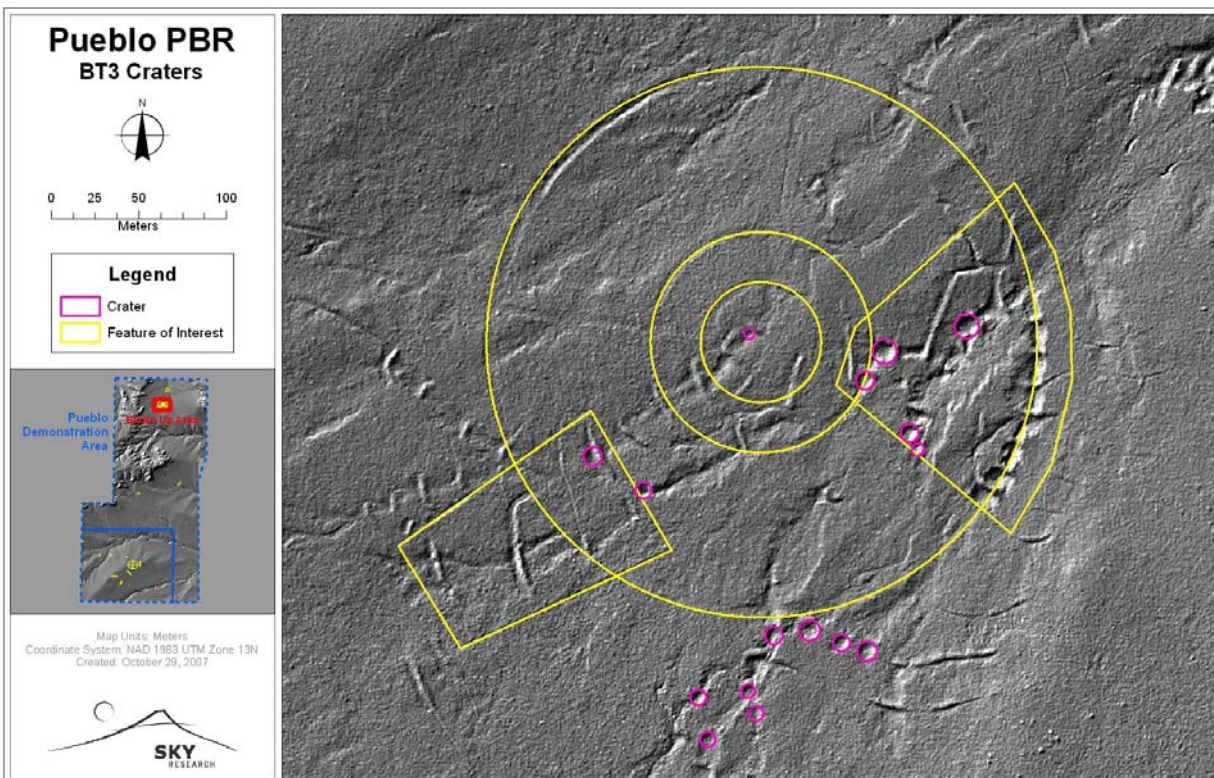


Figure 26. Potential craters detected at BT3.

4.3.2.2 BT4

More than 1,000 potential craters were detected in the vicinity of BT4 (Figure 26). These features were distributed asymmetrically across the study area, with concentrations primarily around the four ship targets. All of the potential craters associated with the BT4 area can be encompassed by a circle with a radius of approximately 1 km, indicating that stray HE rounds associated with the ship targets may be found as much as 1 km away from the center of the target

area. Crater densities exceeded 30 potential craters/hectare around each ship target and dropped to below 5 per hectare in the areas in between the ship targets (Figure 27). No crater-like features were detected inside the 1000 ft aiming circle. This provides evidence that the circular target may have been cleared and graded sometime after HE bombs were dropped.

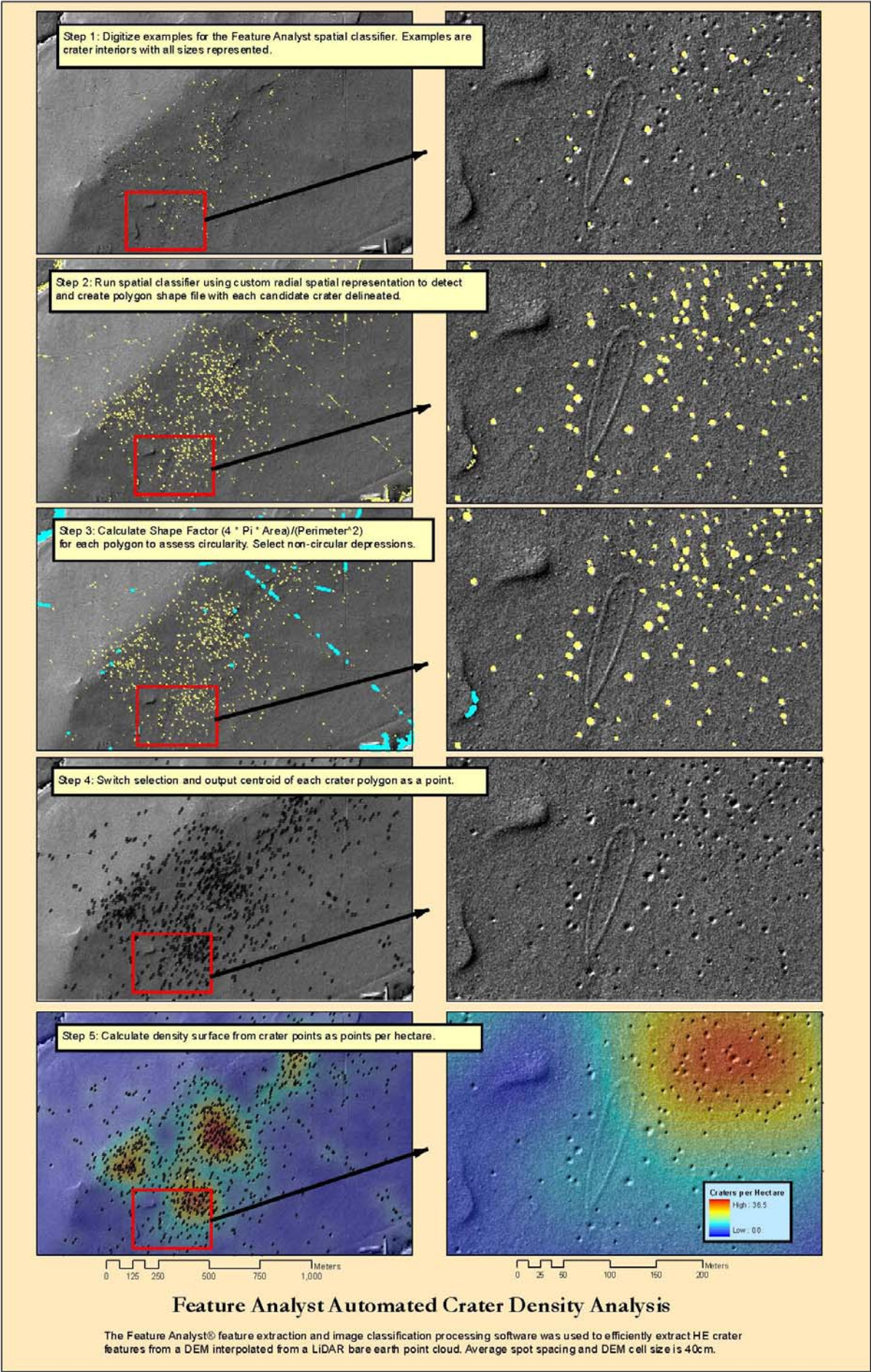


Figure 27. Potential crater density analysis at BT4.

The distribution pattern provides information about the sequence and timing of ordnance use on the site, since the construction (or reconstruction for sonic scoring) of the target circle at BT4 postdates the potential craters associated with HE activity that were detected around the four ship targets. The clearance of the BT4 target circle during the active use of the site also indicates the potential for undocumented disposal or open burn/open detonation (OB/OD) sites nearby.

4.3.2.3 75 mm Suspected Target

No HE cratering was evident in the suspected 75 mm target vicinity.

4.3.3 Range Infrastructure Detection

Range infrastructure features detected in the LiDAR and orthophotography imagery included transportation routes, structures and raised features (Figure 28). The transport routes were extracted from the LiDAR data; these transport routes may have been associated with the former range use or may be related to current ranching activities. A structure feature observable in the orthophotography data in the center of the demonstration area is a ranch building probably unrelated to former range operations. The foundation pad feature (a total of two were found in the imagery) may be a generator pad associated with BT4 that may possibly be related to the sonic scoring infrastructure known to have been implemented on some of the Pueblo PBR#2 bombing targets.

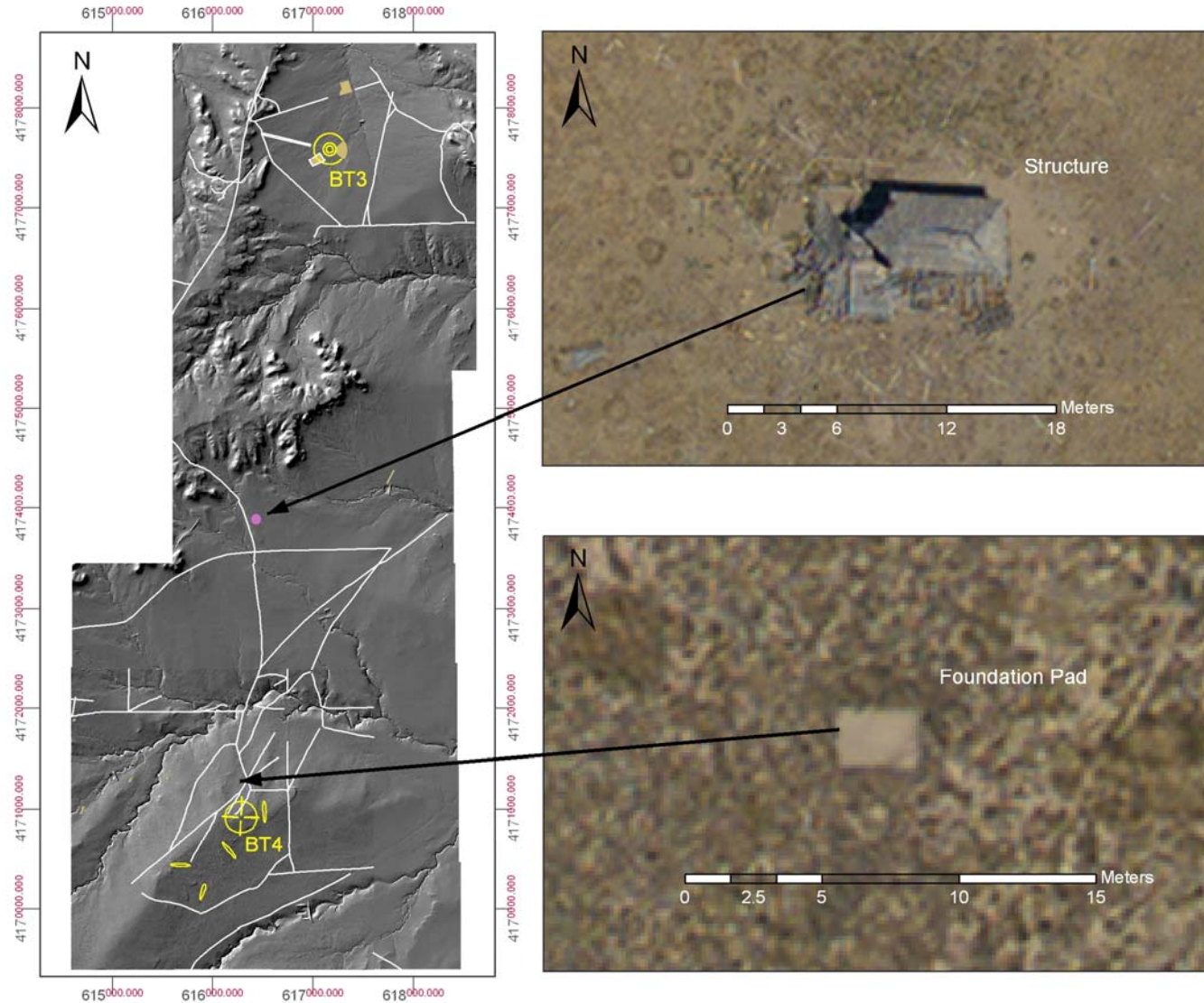


Figure 28. Possible range infrastructure features detected in the imagery includes transport routes (white lines); building structure and foundation pad.

4.4 Performance Criteria

The performance of the high airborne remote sensing technologies was measured against the criteria listed in Table 10.

Table 10. Performance Criteria

Performance Criteria	Description	Type of Performance Objective
Ease of use and efficiency of operations for each sensor system	Efficiency and ease of use meets design specifications	Primary/Qualitative
Georeference position accuracy for each sensor system:	Georeference position accuracy for each sensor system	Primary/Quantitative
Target Area Detection	Comparison of ortho and LiDAR data analysis results with validation data	Primary/Quantitative
Crater Detection	Comparison of LiDAR data analysis results with validation data	Secondary/Quantitative
Range Infrastructure Detection	Comparison of ortho and LiDAR data analysis results with validation data	Secondary/Quantitative

4.5 Performance Confirmation Methods

Table 11 details the confirmation methods that were used for each criterion, the expected performance and the performance achieved.

Table 11. Performance Confirmation Methods and Results

Performance Metric	Confirmation Method	Expected Performance	Performance Achieved
Technology Usage	Field experience using technology during demonstration	Efficiency and ease of use meets design specifications	Pass
Georeference accuracy	Georeference position accuracy for each sensor system	LiDAR: Vertical accuracy - 15 cm RMSE Horizontal accuracy - 40 cm RMSE	Vertical accuracy: Phase I: 11.1 cm Phase II: 3.2 cm Horizontal accuracy: Phase I: 28.2 cm Phase II: 8.5 cm
		Orthophotography: Horizontal accuracy - 40 cm RMSE	Phase I: 28.6 cm Phase II: 26.8 cm
Target Area Detection	Comparison of ortho and LiDAR data analysis results with validation data	>0.90	BT3 and BT4 target areas detected. No target identified at Suspected 75 mm Target Area and confirmed by absence of target evidence during validation surveys.
Crater Detection	Comparison of LiDAR data analysis results with validation data	>0.75 (craters <1m) >0.90 (craters >1 m)	Craters <1m: Found to be not within detection limits. Craters >1m: .90 detection.
Range Infrastructure Detection	Comparison of ortho and LiDAR datasets with validation data	>0.90	N/A

4.5.1 Technology Usage

The use of LiDAR and orthophotography in a high airborne, fixed-wing aircraft is an efficient means for collecting data over large survey areas. The LiDAR sensor and digital camera utilized for this demonstration are easy to operate. The standardized data processing and analysis methodologies are well understood and easy to use for experienced remote sensing analysts.

4.5.2 Georeference Accuracy

The demonstration met the expected georeference accuracies specified in the demonstration design.

4.5.3 Target Area Detection

The validation surveys confirmed the identification and location of BT3 and BT4. The validation surveys confirmed the identification and location of BT4 and the ship targets. The surveys did not find evidence of a target area in the suspected 75 mm Target Area, confirming the findings of the LiDAR and orthophotography analysis.

4.5.4 Detection of Potential Craters

The performance criteria originally developed for the performance assessment were as follows: 70% of craters less than 1 m in diameter were expected to be detected and 90% of potential craters greater than 1 m in diameter were expected to be detected. However, during the crater analysis conducted as part of this project, the results indicated that crater-like features smaller than 1 m in diameter were not detectable in LiDAR imagery (see Section 4.1). Therefore, no value is reported for detection of potential craters smaller than 1 m.

For possible craters detected during the analysis of the LiDAR imagery, validation surveys were used to reacquire the coordinates of 28 craters. These features were then described and identified as a circular depression (i.e., verified as a possible crater) or not. In addition, two craters were identified during the validation surveys that were not identified during the data analysis (validation survey IDs P-005 and P-006); and one possible crater was found to be a linear depression between berms (validation survey ID P-017). These results are reported in Table 12. Therefore, calculation of the performance of the technology to detect craters is the correct identification of 27 out of 30 possible craters, or 90% detection.

4.5.5 Range Infrastructure Detection

The range infrastructure visited during the validation survey was not sufficient to calculate a meaningful detection estimate; therefore, no value is reported for these criteria.

Table 12. Crater Detection Comparison to Validation Data

Area	ID	Description from Validation Survey	Diameter (Validation Survey, in m)	Depth (Validation Survey, in cm)	Identified From LiDAR Analysis?
BT3	P-005	Circular depression	7	60	No
BT3	P-006	Circular depression	5.5	~90	No
BT3	P-007	Roughly circular depression	9.5-10	~85	Yes
BT3	P-008	Roughly circular depression	7.7	70	Yes
BT3	P-009	Roughly circular depression	9	~60	Yes
BT3	P-010	Roughly circular depression	7.5	not reported	Yes
BT3	P-011	Roughly circular depression	9	~50	Yes
BT3	P-012	Roughly circular depression	8.6	~50	Yes
BT3	P-013	Almost perfectly circular depression	10.6	~60	Yes
BT3	P-014	Roughly circular depression	~10-10.5	not reported	Yes
BT3	P-015	Roughly circular depression	~5	35	Yes
BT3	P-016	Elongated depression	7.5	120	Yes
BT3	P-017	Linear depression between berms; not a crater	6.5	~40	Yes
BT3	P-018	Roughly circular depression	1.5	130	Yes
BT3	P-019	Roughly circular depression	12	~100	Yes
BT3	P-020	Roughly circular depression	9.7	90	Yes
BT3	P-021	Roughly circular depression	9	~90	Yes

Area	ID	Description from Validation Survey	Diameter (Validation Survey, in m)	Depth (Validation Survey, in cm)	Identified From LiDAR Analysis?
BT3	P-022	Very roughly circular depression	7	~70	Yes
BT-4	P-028	Circular depression	8	40	Yes
BT-4	P-029	Circular depression	5	~35	Yes
BT-4	P-030	Deep, steep-walled pit	4.7	90	Yes
BT-4	P-031	Broad, shallow circular depression	8	40	Yes
BT-4	P-032	Nearly circular depression	6-6.5	50	Yes
BT-4	P-033	Small, shallow depression	4	~30	Yes
BT-4	P-034	Shallow depression	~6	~35	Yes
BT-4	P-035	Small, shallow depression	3.5	35	Yes
BT-4	P-036	Small, circular depression	4.3	~30	Yes
BT-4	P-037	Circular depression	6	~60	Yes
BT-4	P-038	Compound crater	5-6.5	~65	Yes
BT-4	P-039	Small depression	4	~35	Yes

5. Cost Assessment

5.1 Cost Reporting

Cost information associated with the demonstration of all airborne technology, as well as associated activities, were tracked and documented before, during, and after the demonstration to provide a basis for determination of the operational costs associated with this technology. For this demonstration, Table 12 (Phase I) and Table 13 (Phase II) contain the cost elements that were tracked and documented for this demonstration. These costs include both operational and capital costs associated with the demonstration design and planning; salary and travel costs for support staff; equipment costs associated with aircraft, sensor and camera, support personnel, and costs associated with the processing, analysis, and interpretation of the results generated by this demonstration.

Table 13. Phase I Cost Tracking

COST CATEGORY	SUB CATEGORY	DETAILS	COSTS (\$)
START-UP COSTS	PRE-DEPLOYMENT AND PLANNING	INCLUDES PLANNING, CONTRACTING, SITE VISIT AND SITE INSPECTION	\$13,205
	MOBILIZATION	PERSONNEL MOBILIZATION, EQUIPMENT MOBILIZATION, AND TRANSPORTATION	\$7,783
OPERATING COSTS	HIGH AIRBORNE SURVEY	DATA ACQUISITION AND ASSOCIATED TASKS, INCLUDING AIRCRAFT OPERATION TIME (5.2 HOURS) AND TWO DAYS OF STAND BY TIME (8	\$22,627

		HOURS)	
DEMOBILIZATION	DEMOBILIZATION	DEMOBILIZATION	\$7,783
DATA PROCESSING	DATA PROCESSING	PROCESSING OF LIDAR AND ORTHOPHOTOGRAPHY DATA	\$25,238
DATA ANALYSIS	DATA ANALYSIS	ANALYSIS OF LIDAR AND ORTHOPHOTOGRAPHY DATA	\$26,045
MANAGEMENT	MANAGEMENT AND REPORTING	PROJECT RELATED MANAGEMENT, REPORTING AND CONTRACTING	\$30,462
TOTAL COSTS			\$133,143
ACRES SURVEYED			6,700
UNIT COST			\$19.87/ACRE

Table 14. Phase II Cost Tracking

COST CATEGORY	SUB CATEGORY	DETAILS	COSTS (\$)
START-UP COSTS	PRE-DEPLOYMENT AND PLANNING	INCLUDES PLANNING, CONTRACTING, SITE VISIT AND SITE INSPECTION	\$11,627

	MOBILIZATION	PERSONNEL MOBILIZATION, EQUIPMENT MOBILIZATION, AND TRANSPORTATION	\$13,734
OPERATING COSTS	HIGH AIRBORNE SURVEY	DATA ACQUISITION AND ASSOCIATED TASKS, INCLUDING 4.2 HOURS OF AIRCRAFT OPERATION TIME	\$30,866
DEMOBILIZATION	DEMOBILIZATION	DEMOBILIZATION	\$6,992
DATA PROCESSING AND ANALYSIS	DATA PROCESSING	PROCESSING OF LIDAR AND ORTHOPHOTOGRAPHY DATA	\$21,417
	DATA ANALYSIS	ANALYSIS OF LIDAR AND ORTHOPHOTOGRAPHY DATA	\$8,407
MANAGEMENT	MANAGEMENT AND REPORTING	PROJECT RELATED MANAGEMENT, REPORTING AND CONTRACTING	\$29,137
TOTAL COSTS			\$122,180.00
ACRES SURVEYED			6,600
UNIT COST			\$18.51/ACRE

5.2 Cost Analysis

A major cost driver for an airborne survey system is the cost of aircraft airtime. In terms of tasks, this constitutes a large percentage of the mobilization, data acquisition and demobilization costs. Mobilization and demobilization costs are generally a function of the distance from the home base for the aircraft, equipment and personnel. For this demonstration, the aircraft mobilized and demobilized between Ashland, Oregon, and the demonstration site, requiring on average 4.5 hours of flight time in each direction. Stand by time also increases the costs; for the Phase I demonstration, two days of stand by were required due to weather. The stand by costs increase the aircraft cost due to minimum daily hour costs (four hour minimums were in effect for this demonstration).

In addition, the cost of equipment (LiDAR sensor, digital camera and GPS equipment) constituted a large percentage of the data acquisition costs for this demonstration. Data processing and analysis functions made up the bulk of the remaining costs associated with the results of the demonstration.

Project management and reporting were a significant cost for this demonstration, as the project was conducted under the WAA-PP and required more meetings, travel and reporting than would generally be expected for a production level survey.

Costs associated with validation were not considered in the cost analysis, as the validation was conducted as part of the WAA-PP.

6. Implementation Issues

6.1 Regulatory and End-User Issues

The ESTCP Program Office has established a WAA-PP Advisory Group to facilitate interactions with the regulatory community and potential end-users of this technology. Members of the Advisory Group include representatives of the US EPA, State regulators, Corps of Engineers officials, and representatives from the services. ESTCP staff has worked with the Advisory Group to define goals for the WAA-PP and develop Project Quality Objectives.

There will be a number of issues to be overcome to allow implementation of WAA beyond the pilot program. Most central is the change in mindset that will be required if the goals of WAA extend from delineating target areas to collecting data that are useful in making decisions about areas where there is not indication of munitions use. A main challenge of the WAA-PP is to collect sufficient data and perform sufficient evaluation that the applicability of these technologies to uncontaminated land and their limitations are well understood and documents. Similarly, demonstrating that WAA data can be used to provide information on target areas regarding boundaries, density and types of munitions to be used for prioritization, cost estimation and planning will require that the error and uncertainties in these parameters are well documented in the program.

7. References

Office of the Under Secretary of Defense for Acquisition, Technology, and Logistics, December 2003, "Report of the Defense Science Board Task Force on Unexploded Ordnance," 20301-3140.

Sky Research, 2007, "Demonstration of Airborne Wide Area Assessment Technologies at Pueblo Precision Bombing Ranges, Colorado," Final Report, ESTCP Project 2000416.

United States Army Corps of Engineers, St. Louis District, 2005, Archive Search Report.

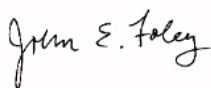
Versar, 2005, "Former Pueblo Precision Bombing Range #2, Conceptual Site Model, V0."

8. Points of Contact

Table 15. Points of Contact

POINT OF CONTACT	ORGANIZATION	PHONE/FAX/EMAIL	ROLE IN PROJECT
DR. JOHN FOLEY	SKY RESEARCH, INC. 445 DEAD INDIAN ROAD ASHLAND, OR 97520	(TEL) 978.479.9519 (FAX) 720.293.9666	PRINCIPAL INVESTIGATOR
MS. STACEY KINGSBURY	SKY RESEARCH, INC. 445 DEAD INDIAN ROAD ASHLAND, OR 97520	(TEL) 540.961.9132 (FAX)	PROJECT MANAGER
MR. JERRY HODGSON	USACE OMAHA DISTRICT 215 N. 17TH STREET OMAHA, NE 68102-4978	(TEL) 402.221.7709 (FAX) 402.221.7838	FEDERAL ADVOCATE
MR. HOLLIS (JAY) BENNETT	US ARMY R&D CENTER (CEERD-EE-C) 3909 HALLS FERRY ROAD VICKSBURG, MS 39180-6199	(TEL) 601.634.3924	DOD SERVICE LIAISON

Project Lead Signature:



Appendix A: Optech ALTM 3100 Specifications

ALTM 3100: 3,500 m altitude! 100,000 laser pulses per second!

ALTM 3100 Specifications

Airborne Module

Operating altitude	80 - 3,500 m nominal
Horizontal accuracy	1/2,000 x altitude; 1 sigma
Elevation accuracy	<15 cm at 1.2 km; 1 sigma <25 cm at 2.0 km; 1 sigma <35 cm at 3.0 km; 1 sigma
Range resolution	1 cm
Range capture	Up to 4 range measurements for each pulse including last
Intensity capture	12 bit dynamic range for each measurement
Scan frequency	Variable; maximum 70 Hz
Scan angle	Variable from 0 to $\pm 25^\circ$, in increments of $\pm 1^\circ$
Scanner Product	Scan angle x scan frequency $\leq 1,000$
Roll compensation	5 Hz update rate (Scan angle + Roll comp. angle = 25° , i.e., $\pm 20^\circ$ scan allows $\pm 5^\circ$ compensation)
Swath width	Variable from 0 to $0.93 \times$ altitude m
Position Orientation System	Applanix - POSAV 510 including Internal 12 channel dual frequency 2 Hz GPS receiver
Spot distribution	Sawtooth, uniform across 96% of scan
Laser repetition rate	33 kHz (max. altitude (AGL) 3.5 km) 50 kHz (max. altitude (AGL) 2.5 km) 70 kHz (max. altitude (AGL) 1.7 km) 100 kHz (max. altitude (AGL) 1.1 km)
Data storage hard drives	Ruggedized removable hard drive Minimum 7 hr. continuous log time @ 100 kHz
Beam divergence	Dual divergence 0.3 mrad (1/e) or 0.8 mrad (1/e)
Laser classification	Class IV (FDA CFR 21)
Power requirements	28 VDC, 35 A (maximum)
Operating temperature (air temperature)	Control rack: $+10^\circ\text{C}$ to $+35^\circ\text{C}$ Sensor head: -10°C to $+35^\circ\text{C}$ (assuming the use of thermal jacket)
Storage temperature	-10°C to $+50^\circ\text{C}$
Humidity	0 - 95% non-condensing



Control Rack

Vibration-isolated case:	
Dimensions/weight (in-flight)	65 cm x 59 cm x 49 cm/53.2 kg covers removed, with removable hard drive installed
Cables/laptop	7.6 kg/3 kg

Sensor Head

Fits standard camera mounts or mounts directly to floor	
Overall dimensions/weight (in-flight)	26 cm x 19 cm x 57 cm/23.4 kg (incl. sensor insulating jacket)
Minimum opening	19.2 cm x 25.5 cm (flight direction)

Processing Software

REALM Survey Suite	Differential kinematic GPS solution Trajectory optimization from multiple base stations XYZ point calculations module Vegetation classification/extraction feature Windows NT/2000/XP compatible
--------------------	--

GPS Ground Support

Multiple base stations	Any dual frequency receiver with Rinex output
------------------------	---

Available Options

4k x 4k Digital camera	Integrated metric frame camera to deliver geo-referenced (X,Y,Z) color or color-IR images with sub-pixel accuracy
Intelligent Waveform Digitizer	8 bits @ 1 nsec sample interval per pulse (maximum 50 kHz)

Note: to meet its stated accuracy, the ALTM must receive GPS data of sufficient quality. GPS data quality shall be viable only when all of the following conditions are met:

- At least four satellites are in lock (tracked by the receiver) throughout the survey
- Elevation of the satellites is good (i.e., PDOP < 4)
- Aircraft stays within 30 km of the GPS base station

If one or more of these conditions is not met, or if any source of electromagnetic interference causes the GPS receivers to repeatedly lose lock, the specified accuracy of the ALTM will be compromised.

Specifications subject to change without notice.

100 Wildcat Road • Toronto, ON • Canada M3J 2Z9

Tel: [416] 661-5904 • Fax: [416] 661-4168

Web: www.optech.on.ca • Email: inquiries@optech.on.ca

© Copyright 2004, Optech Incorporated. All rights reserved. 270104



Appendix B: ALTM 4K X 4K Digital Camera Specifications

ALTM 4K02 - The Digital Image Collection and Processing Solution

Specifications

Camera

Array size	4,092 (along flight) x 4,079 (cross flight) pixels
Pixel size	0.009 mm
Premium grade CCD*	Point defects <= 2000 Cluster defects <= 30 Single column Defects <=10 Dead columns = none Radiometric and geometric profile included
Filter array	Interchangeable color or color-IR
Lens	Zeiss Distagon 55.0 mm, 36° FOV
Exposure control	Automatic: aperture or shutter priority
Shutter	Electronically controlled focal plane
Shutter speed	1/125 - 1/4,000 seconds
Exposure compensation	± 2 EV in 1/3 EV steps
Exposure rate	Maximum 4 seconds**
Housing	Proprietary ruggedized and individually profiled CCD array mount. Ruggedized exoskeleton, capable of <1 pixel geometric accuracy over RTCA/DO-160D shock and vibration
Calibration	Terrestrial and airborne calibration with full report
Modular replaceability	Includes spare exoskeleton, pre-calibrated camera body and lens for instant field servicing

Ruggedized Data Recorder

- Integrated with ALTM control rack
- Internal pressurized 80 GB disk
- Removable 80 GB disks (2)
- Mission planning & camera trigger via ALTM-NAV
- QC thumbnail image display on ALTM-NAV

Image Performance

Typical at 1,500 m, 120 knots and 1/2,000 exp.

GSD: 0.25 m
Smear: 15%

Bands	1	2	3
Color Mode, nm	400-500	500-600	600-680
CIR mode, nm	510-600	600-720	720-800

Physical

Size	Camera	16 x 18 x 41 cm
	Data recorder	19" rack, 3U height
Weight	Camera	5 kg
	Data recorder	10 kg
Power	Camera/data recorder	28 VDC, 4 A
	Auxiliary power unit	115 VAC
Operating temperature	0 to + 40° C	
Humidity	5 to 90% RH non-condensing	
Altitude	maximum 6,000 m	

Processing Software (included)

MissionVue - downloads images from removable drives

ImageVue - develops digital image

- Applies fall-off corrections and color balance
- Formats: TIFF, JPEG, IMG
- Quantization: 8 or 16 bit

POS Cal and POS EO from Applanix Corp.

ImageStation Suite from Z/I Imaging

- ISAT Aerial Triangulation Software***

Option

- OrthoPro/Geomedia for orthorectification and mosaicing

Specifications subject to change without notice.

*Specially selected from Class 1 (see Kodak KAF-16801CE.V4.pdf)

**Two seconds available in a future release

***Microstation not supplied



Images: Camera and Data Recorder



100 Wildcat Road • Toronto, ON • Canada M3J 2Z9

Tel: [416] 661-5904 • Fax: [416] 661-4168

Web: www.optech.on.ca • Email: inquiries@optech.on.ca

© Copyright 2004, Optech Incorporated. All rights reserved. 090204



Appendix C: Feature Database and Attribute Summary

Table C-1. Feature Dataset and Attribute Summary

Feature Dataset - CSMV1_datasets.mdb	Description
AREA_OF_INTEREST_CSMV1 (schema only)	Advanced analysis models integrating all high airborne remote sensing datasets
CRATERING_FEATURE	Craters and depressions on site
FEATURE_OF_INTEREST_CSMV1	Potential targeting and range infrastructure features associated with UXO activities
INFRASTRUCTURE_CORRIDORS	Corridor features found in the orthophotography and LiDAR datasets including historic and current roads, power lines, railways, and fences
MASK_AREAS_CSMV1	Areas eliminated from the analysis due to environmental factors or insufficient sensor coverage